Optimization of Centrifugal Slurry Pump Through the Splitter Blades Position

Ehsan Abdolahnejad
Iran University of Science and Technology
Mahdi Moghimi (moghimi@iust.ac.ir)
Iran University of Science and Technology https://orcid.org/0000-0002-5450-3338
Shahram Derakhshan
Iran University of Science and Technology

Original Article

Keywords: Slip factor, Splitter blade, Slurry pump, CFD, Experimental test

Posted Date: January 29th, 2021

DOI: https://doi.org/10.21203/rs.3.rs-155416/v1

Version of Record: A version of this preprint was published at Proceedings of the Institution of Mechanical Engineers, Part C: Journal of Mechanical Engineering Science on October 1st, 2021. See the published version at https://doi.org/10.1177/09544062211027608.

Optimization of centrifugal slurry pump through the splitter blades position

Ehsan Abdolahnejad, Mehdi Moghimi*, Shahram Derakhshan
Iran University of Science & Technology, School of Mechanical Engineering, Narmak, Tehran 16844, Iran

Abstract
Optimal transfer of two-phase solid-liquid flow (slurry flow) has long been a major industrial challenge. Slurry pumps are among the most common types of centrifugal pumps used to deal with this transfer issue. The approach of improving slurry pumps and consequently increasing the efficiency of a flow transmission system requires overcoming the effects of slurry flow such as the reduction in head, efficiency, and wear. This study attempts to investigate the changes in the pump head by modifying the slip factor distribution in the impeller channel. For this purpose, the effect of splitter blades on slip factor distribution to improve the pump head was investigated using numerical simulation tools and validated based on experimental test data. Next, an optimization process was used to determine the characteristics of the splitter (i.e., length, number, and environmental position of the splitter) based on a combination of experimental design methods, surface response, and genetic algorithm. The optimization results indicate that the splitters were in a relative circumferential position of 67.2% to the suction surface of the main blade. Also, the optimal number and length of splitter blades were 6 and 62.8% of the length of the main blades, respectively. Because of adding splitter blades and the reduction in the flow passage, the best efficiency point (BEP) of the slurry pump moved toward lower flow rates. The result of splitter optimization was the increase in pump head from 29.7 m to 31.7 m and the upkeep of efficiency in the initial values.
Keywords: Slip factor; Splitter blade; Slurry pump; CFD; Experimental test

Introduction

Centrifugal pumps are among the most widely used turbomachines for transferring fluid in various industries. One of these applications is a two-phase solid-liquid (slurry) flow transfer, which is commonly used in food, mineral, and chemical industries. Centrifugal pumps account for approximately 20% of the world's total energy consumption and about 25 to 50% of industrial energy consumption (Hydraulic Institute et al., 2001). Consequently, many studies have been conducted to improve their performance. Nowadays, the calculation power development of computers has made it possible to expand the traditional design methods through new approaches, optimization algorithms, and computational fluid dynamics (CFD). This development has reduced the time and money spent on achieving the optimal design.

Optimization methods are generally divided into gradient-based and evolutionary methods (Haslinger & Mäkinen, 2003). In the former, the slope of the objective function is calculated, followed by discovering the local optimal solutions. Nevertheless, this method is possible unable to find the global optimal solution. Various studies have been conducted to develop these methods (Derakhshan et al., 2008, 2009, 2010). The latter, however, is pertinent to search methods based on the value of the objective function in the entire solution domain; thus, it can find the absolute optimal value. Evolutionary optimization methods can optimize several objective functions simultaneously (G. G. Wang & Shan, 2007).

Reducing the head and increasing the wear are two significant effects of slurry flow on centrifugal pumps' performance. Finding a solution to increase the pump head while maintaining its efficiency requires an optimization process. The beginning of this process requires determining the relationship between impeller geometry parameters and performance characteristics such as head and efficiency. Typically, there are two means to achieve performance parameters: experiments and numerical simulations. The results obtained from either numerical methods or experimental tests can be used in the iterative process for optimization unless a proper metamodel is built between the design inputs and the target functions.

A metamodel appraises the function between input and output that guarantees using a simulation model. Metamodels also are known as response surfaces, emulators, auxiliary models, and surrogates (Kleijnen, 2009). Since optimization is generally used in combination with surrogate methods by applying evolutionary methods in nonlinear problems, they are known as surrogated-assisted evolutionary optimization (Y. Jin, 2011). Surrogate methods in each problem are responsible for finding the relationship between input and output and generating the database required for performing the optimization process (Bandler et al., 2004).

In recent decades, extensive research has been devoted to developing optimization methods and achieving sustainable optimal design methods for centrifugal pumps (Lu et al., 2018). Nourbakhsh et al. (2011) compared particle swarm optimization (PSO) and non-dominated sorting genetic algorithm-II (NSGA-II) methods. The results showed that the former has higher and better accuracy in determining the numerical solution borders CFD. Optimizing the impeller geometry using a combination of artificial neural networks (ANNs) and artificial bee colony (ABC) algorithm was accomplished by Derakhshan et al. (2013) on a centrifugal pump. They showed that using ANNs reduced the quantity, time, and cost of CFD solutions, as well as improving the efficiency and head by about 3.59% and 6.89 meters, respectively. Zheng et al. (2014) used two optimization methods for a multi-objective optimization problem. The

NSGA-II and another evolutionary algorithm based on decomposition (MOEA/D) were employed to solve the optimization problem. Based on the obtained results, the MOEA/D algorithm is more accurate than the NSGA-II model. In addition to ANN, the response surface method (RSM) is utilized as a surrogate model in combination with sample selection models such as the design of experiment (DOE) in the turbomachine optimization process. Using these methods increases speed and decreases the costs of optimization (Pei et al., 2017). A review on the use of surrogate models in optimization applications was presented by Wang & Shan (2007).

The metamodel-based optimization can assess the response function behavior more accurately compared to other optimization approaches, because of the low computational costs involved (Y. Zhang et al., 2014). Regarding such lower computational costs in using response surface methods, several studies have been carried out. For instance, Zhang et al. (2014) utilized a multi-objective optimization model for a two-suction pump using the Kriging metamodels as an alternative method. Pei et al. (2016) applied a combination of SRM and NSGA-II to a multi-objective optimization problem concerning a centrifugal pump to achieve a wider operating range. Wang et al. (2016) compared three different models of surrogate methods, namely RSM, Kriging, and radial basis function (RBF) neural network. The results revealed that RSM had the highest efficiency. Suh et al. (2019) used the response surface surrogate model to address the optimization of suction nozzle performance in a mixed flow pump.

In recent years, numerous studies have been conducted in this field (Wenjie Wang et al. 2017, 2019). Among the introduced surrogate metamodels, the Kriging model is less used in the design of centrifugal pumps. Providing an unbiased prediction for unknown response points is a significant advantage of this model compared to the other ones (Martin, 2009).

In this study, the head and efficiency of a splitter-type impeller with relative opposite changes are optimized. To this aim, a robust multi-objective optimization algorithm is needed to cover the whole solution domain and find the whole set of Pareto solutions. Evolutionary algorithms (EAs) are the best option for finding Pareto solutions. In this study, the genetic algorithm (GA), as one of the most well-known algorithms in this regard, was employed.

As mentioned, one of the most critical issues in pumps is the reduction of the pump head in slurry application compared to fluid water. Abrasion is commonly regarded as an essential factor in the useful life of slurry pumps. The impeller blades are responsible for transferring energy to the fluid and directing the flow. Theoretically, the increase in the number of blades in spearheads leads to better performance in directing the flow (Gülich, 2010). Moreover, the solid particles in the slurry increase the abrasion rate in the blades. Meanwhile, using more blades increases the abrasion and friction, as well as blocking the flow channel. On the other hand, reducing the number of blades increases the deviation between blades and flow direction, as well as reducing the slip factor and the produced head (Gülich, 2010). Hence, lowering the number of main blades and adding the splitter blades, as much as possible, is the optimum approach selected between the two solutions. In this respect, in addition to properly directing the flow and stabilizing the slip factor, the contact surface between the flow and the blade wall is reduced.

Several studies have been conducted on adding splitter blades to the impeller of centrifugal pumps. Gui et al. (1989) investigated the effect of splitter blades on the performance of a radial fan with forward blades. Experimental tests showed that the peripheral position of the splitter

blades has a significant effect on the performance of the radial fan. In this methodology, approaching the splitter blades to the pressure side of the main blades improves the head and their approach to the suction pressure side of the main blades improves the efficiency slightly. Miyamoto et al. (1992) conducted an experimental study on the effect of splitter blades on pressure distribution and flow phenomena in two types of shrouded and unshrouded impellers. The results indicated an improvement in tangential velocities and total pressure. Gölcü (2006) investigated the effect of splitter blade length and number of main blades on the performance characteristics of a deep well pump using the ANN. Kergourlay et al. (2007) investigated the effect of splitter blades on the flow field of a centrifugal pump in a comparative experimental analysis. They studied the slip factor as a parameter affected by flow direction and showed that adding splitter blades improves the head. Moreover, adding blades increase the interaction between the impeller and the cutwater, as well as increasing the radial forces. Heo et al. (2015) optimized an axial fan by adding a splitter and using the response surface approximation model. Cavazzini et al. (2015) evaluated the impact of splitter blades on suction nozzle performance by conducting an experimental and numerical investigation. Adding splitter blades in the suction nuzzle, in the case of high flow rates, improved the cavitation behavior, but it slightly increased the NPSH at low flow rates. Korkmaz et al. (2017) investigated the changes in the performance of a well pump in the presence of splitter blades of different lengths and numbers. The results demonstrate the possibility of improving the efficiency and head using splitter blades, especially for pumps with low specific speed. In their study, the optimal length of the splitter blades was obtained between 0.7 and 0.85 of the main blades' length. Yuan et al. (2017) examined the effect of splitter blade length and their inlet angle on the performance of high-speed centrifugal pumps. The results did not show a significant impact on the head and efficiency. Li et al. (2018) investigated the internal flow behavior during pump operation, with and without splitter blades, in a turbine pump. They showed that the addition of splitter blades increased the head and efficiency by 2 m and 2.4%, respectively. Khoeini and Tavakoli (2018) studied the optimal position of the splitter blades in a diffuser pump. They added splitter blades in five distinct positions and assessed the head and efficiency characteristics. Consistent with the results, the efficiency improved slightly by about 1.7%, as the splitter blades approached the main blades' suction side. Also, setting the splitter blades in the middle of the channel led to better head results. Zhang et al. (2018) investigated the peripheral position of the splitter blades and its effect on the pump head and efficiency. According to their results, such a system effectively improves the mentioned characteristics. When the outlet edge of the splitter blades approached the suction side of the main blade by 12°, both the head and efficiency were enhanced. This result is in contrast with the study of Gui et al. (1989) and thus requires further study. Namazizadeh et al. (2020) investigated the effect of the peripheral position of the splitter blades on the head and efficiency. The results show that the efficiency values are higher when the splitter is close to the suction side. However, an increase in the head was observed when the splitter blade was in the middle or slightly closer to the pressure level. As a general upshot, the splitter blades affect the head more than the efficiency. Torre et al. (2018) optimized the position and profile of splitter blades in a centrifugal pump using the response surface surrogate model and non-linear programming by quadratic Lagrangian (NLPQL). The results indicate a 2% and 4.7% increase in the head and performance range without cavitation.

Based on the research background, most of the related studies have been carried out on splitter blades for water fluid to investigate changes in the pump head and efficiency as research objectives. This study investigates adding splitter blades to a centrifugal pump impeller in the presence of slurry flow. The effect of splitter blades on the correction of slip factor distribution is considered an effective parameter in producing head by the pump. In this regard, reducing the number of main blades and using splitter blades leads to head improvement in addition to the slip factor distribution. Also, to achieve the optimal geometry of the splitters, the surrogate Kriging model is employed in the optimization method.

The slurry flow studied in this research consists of water and glass beads. This flow has a greater effect on reducing the head in centrifugal pumps than the non-Newtonian kaolin slurries studied by the authors hitherto.

Determining the splitters' optimum peripheral position, the length of the blades, and the number of splitter blades requires an optimization process. In the present study, the splitter blades are optimized by combining the response surface surrogate method and GA with the DOE sample selection technique (Y. Jin, 2011). Also, the slip factor distribution in two cases, before and after adding splitter blades, is explored and compared. An experimental test was performed to complete the study and validate the numerical solutions. Eventually, the validated solution is used for flow analysis and optimization.

2- Optimization methodology

This research aims at improving the head in a centrifugal pump by focusing on correcting the slip factor distribution in the impeller channel by adding splitter blades. The objective function is considered the maximum head while maintaining the initial efficiency. The optimal impeller geometry is attained based on these two objectives. Fig. 1 depicts the optimization process.

To optimize this problem, first, the initial geometry is parameterized without the splitter blades, and then a new impeller is parameterized based on the splitter characteristics. Afterward, according to the range of variations in each design variable, sampling is performed based on the LHS experimental design sampling method. In the third step, the relationship between the inputs and outputs of the problem is obtained using the response surface surrogate method based on the Kriging model. Finally, the optimization process is performed using the GA, and the optimal values of the splitter design variables are calculated with respect to the objective function.

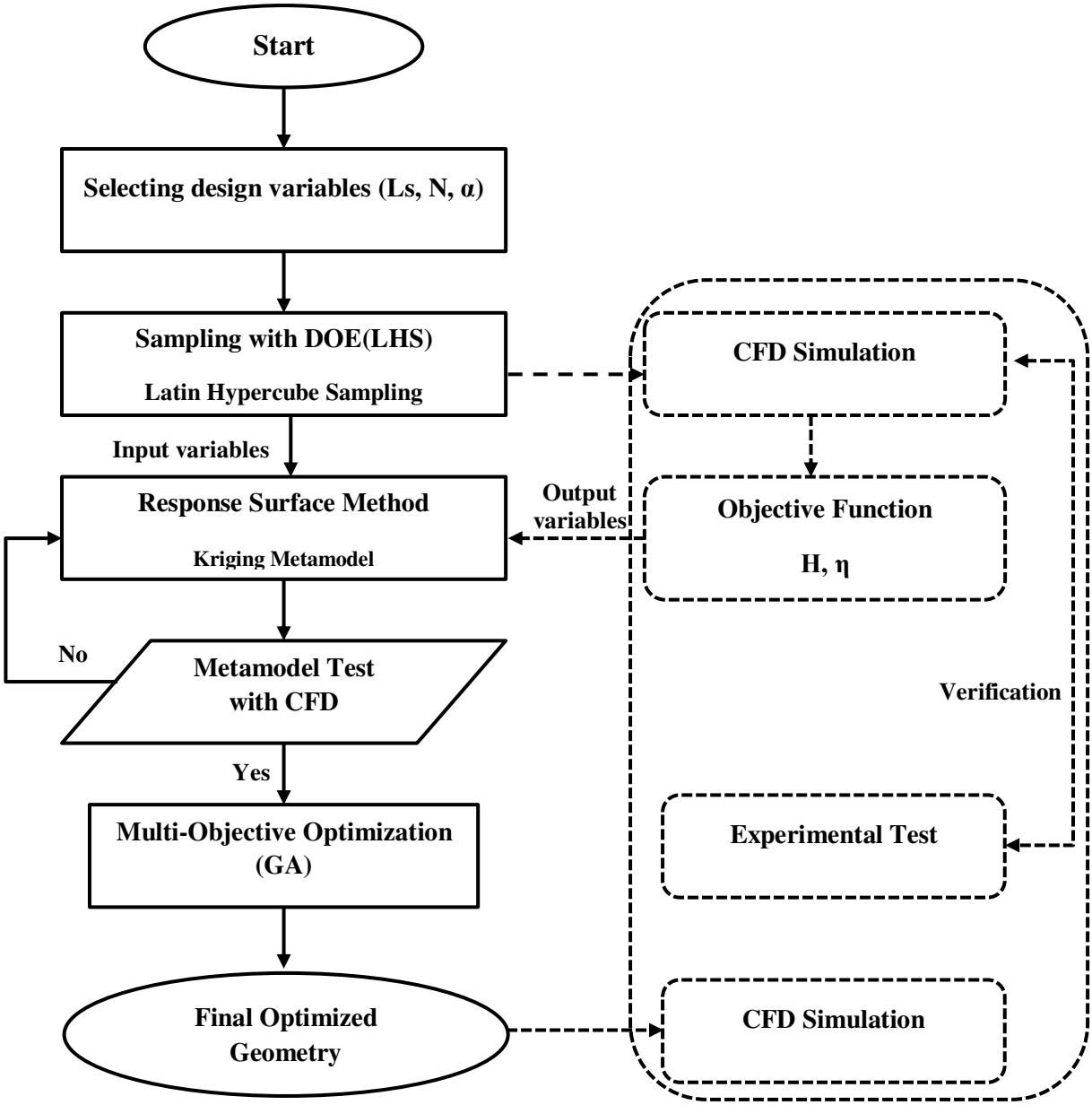

Fig. 1. Flow diagram of the optimization

3- Numerical simulation

The Euler-Euler and the Euler-Lagrange are two fundamental approaches in CFD modeling of multiphase flow. For the current case study, the Euler-Euler approach was selected, based on flow properties such as particle loading, dispersed phase volume fraction, Stokes number, and particle relaxation time. As can be seen from Table 1, the Stokes number is defined as the relation between the particle response time and that of the system (Crowe et al., 2012). Interfacial momentum transfer is modeled by applying the free surface model (Hirt & Nichols, 1981), mixture model (Manninen & Taivassalo, 1996), and algebraic slip model (particle model) (Pericleous & Drake, 1986).

Among the mentioned models, for example, the last two are appropriate for modeling the dispersed phase in the continuous phase and sand in water. In the present study, the algebraic slip model (ASM) is utilized for GBW slurry, considering particle concentration and size.

Table 1. Properties of the simulated flows

Flow	Slurry type	Volumetric concentration (%)	Particle shape/size (μm)	Flow density (kg/m3)	Particle loading $PL=\alpha_S\rho_S/\alpha_C\rho_C$	Particulate Stokes number
Water	-	-	-	997	-	-
GBWslurry	Newtonian Inhomogeneous	5.6	Spherical/ $d_{60\%}$=90.0	1082	0.1	0.18
		10.0		1150	0.15	0.18

3-1- Governing equations and turbulence modeling

Governing equations for single-phase case are continuity and momentum equations, which are expressed by Eqs. (1) and (2), respectively.

$$\frac{\partial}{\partial t}(\rho)+\nabla.(\rho U)=0\ , \tag{1}$$

$$\frac{\partial}{\partial t}(\rho U)+\nabla.\left(\rho U\otimes U-\mu\left(\nabla U+(\nabla U)^{T}\right)\right)=-\nabla p \tag{2}$$

Various phase components are dispersed in continuous substrate based on the ASM postulate. According to ASM, a single fluid is defined by incorporating continuous and dispersed phases. The concentration and transport equations represent that in each dispersed phase relative movement in the single fluid is allowed with the transport equation. It is worth noting that the quasi-steady state is considered to local conditions for the dispersed phase. In this equation, phase slip is defined as drift or mutual movement of the dispersed phase. Regardless of the outputs of full partial differential equations, the local variables are used to calculate the slip velocity. Moreover, it is supposed that only the drag force creates an interphase momentum transfer. The ASM requires relaxation time for the dispersed phase to be short compared with changes in the flow, i.e., the Stokes number < < 1 (See supplementary material S1).

Therefore, the model is suitable for simulating the separation of particles or droplets under the influence of gravity, centrifugal force, or some other body forces (Ishii, 1975; M.; Manninen et al., 1996).

The phasic momentum equation in multiphase flow (for phase α and volume fraction r_α) is expressed as:

$$\rho_\alpha r_\alpha\frac{\partial u_\alpha^i}{\partial t}+\rho_\alpha r_\alpha u_\alpha^j\frac{\partial u_\alpha^i}{\partial x^j}=-r_\alpha\frac{\partial p}{\partial x^i}+\frac{\partial\left(r_\alpha\tau_\alpha^{ji}\right)}{\partial x^j}+r_\alpha\rho_\alpha g^i+M_\alpha^i \tag{3}$$

where M_α^i denotes the momentum transfer with other phases. The bulk momentum equation is:

$$\frac{\partial\left(\rho_m u_m^i\right)}{\partial t}+\frac{\partial\left(\rho_m u_m^j u_m^i\right)}{\partial x^j}=-\frac{\partial P}{\partial x^i}+\frac{\partial\left(\tau_m^{ji}+\tau_D^{ji}\right)}{\partial x^j}+\rho_m g^i \tag{4}$$

where

$$\rho_m = \sum_\alpha r_\alpha \rho_\alpha$$
$$\rho_m u_m^i = \sum_\alpha r_\alpha \rho_\alpha u_\alpha^i$$
$$\tau_m = \sum_\alpha r_\alpha \tau_\alpha \quad (5)$$
$$\tau_D^{ji} = -\sum_\alpha r_\alpha \rho_\alpha \left(u_\alpha^i - u_m^i\right) u_\alpha^j$$

Combining these bulk equations with the phasic momentum equations and performing some assumptions lead to interphase momentum transfer M_α^i as follows:

$$M_\alpha^i = r_\alpha \left(\rho_\alpha - \rho_m\right)\left(\frac{\partial u_m^i}{\partial t} + u_m^j \frac{\partial u_m^i}{\partial x^j} - g^i\right) \quad (6)$$

Moreover, interphase momentum transfer is only due to drag and that the particles are spherical. Then,

$$M_\alpha^i = -\frac{3}{4}\frac{r_\alpha \rho_c}{d_p} C_D \left|u_{S\alpha}\right| u_{S\alpha}^i \quad (7)$$

which leads to the following closed relationship for the slip velocity:

$$\left|u_{S\alpha}\right| u_{S\alpha}^i = -\frac{4}{3}\frac{d_p}{\rho_c C_D}\left(\rho_\alpha - \rho_m\right)\left(\frac{\partial u_m^i}{\partial t} + u_m^j \frac{\partial u_m^i}{\partial x^j} - g^i\right), \quad (8)$$

where the slip and the drift velocity are defined as:

$$u_{S\alpha}^i = u_\alpha^i - u_c^i$$
$$u_{D\alpha}^i = u_\alpha^i - u_m^i \quad (9)$$

Also, drag force based on Schiller and Naumann (Schiller & Naumann, 1935) is as follow:

$$C_D = \begin{cases} 24\left(1 + 0.15\,\mathrm{Re}^{0.687}\right)/\mathrm{Re} & \mathrm{Re} \le 1000 \\ 0.44 & \mathrm{Re} \ge 1000 \end{cases} \quad (10)$$

The k-ε model is mostly utilized for turbulence modeling (Caridad & Kenyery, 2004; Nabil et al., 2013; Ofei & Ismail, 2016; Suh et al., 2018; Wu et al., 2015).

3-2- Geometry and boundary condition

A single-stage horizontal centrifugal pump selected as the case study. The solution domain was divided into five parts: Pump inlet, front and rear chambers, impeller, and volute (Fig.2 (a)). Numerical solution was done in steady state condition. Constant velocity at impeller inlet and constant pressure at the volute outlet was considered as a boundary condition. The flow was considered to be incompressible, and fluid properties are constant. The no-slip boundary condition is applied at the impeller and volute casing walls. A turbulence intensity of 5% is imposed at the inlet section. The calculations assume a rotationally periodic boundary condition

on impeller, while the frozen rotor technique is used to model the interaction between the pump impeller and its surrounding volute casing.

3-3- Computational domain mesh independency

The structured hexahedral grid in the solution domain was generated and the independence of the pump's head from grid number is checked for GBW slurry as depicted in Fig. 2 (b). As can be seen, the efficiency varies by less than 0.5% when grid numbers are more than 1.5 million.

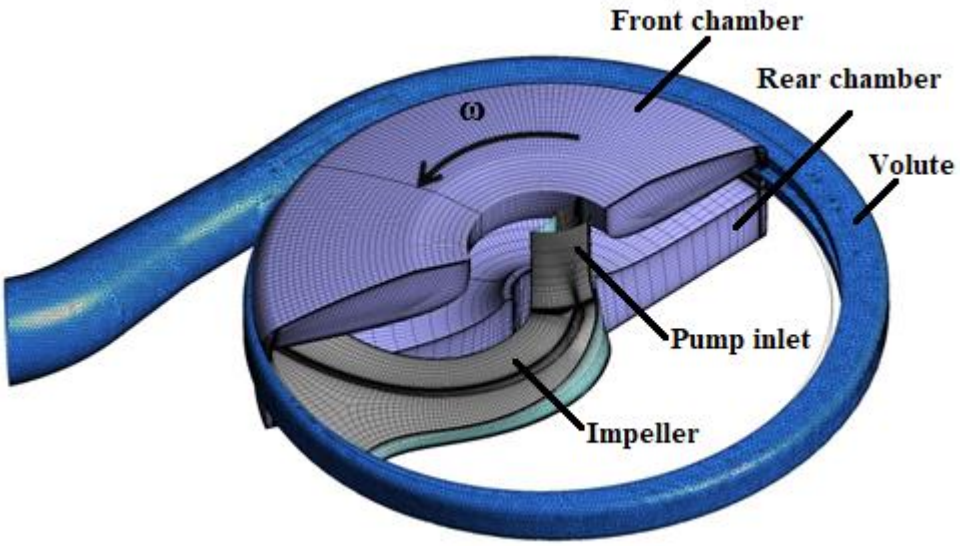

Fig. 2(a). Final generated mesh for the complete computational domain

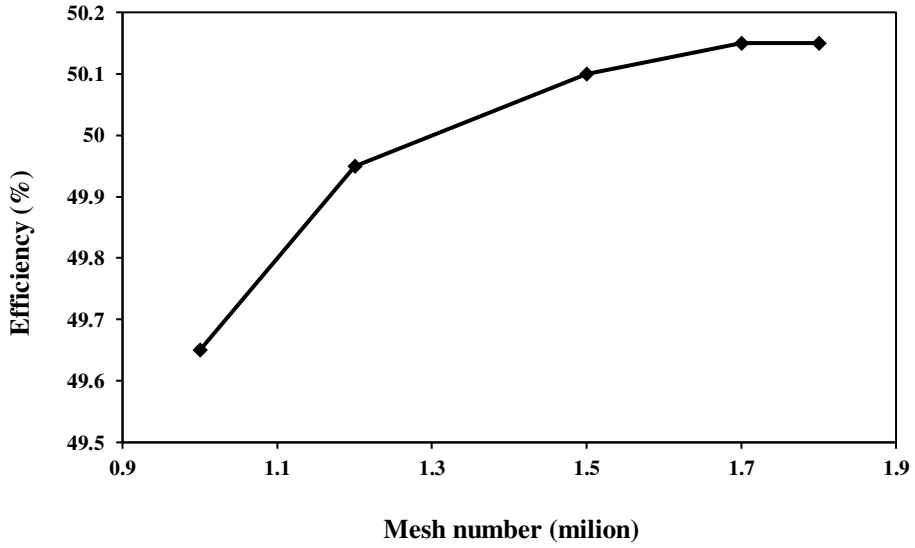

Fig. 2(b). Mesh independency for the complete computational domain

3-4- Slip factor

The amount of energy that a centrifugal pump can transfer to the fluid is calculated by the Euler

equation (Eq. 11) .

$$H_{T\infty} = \frac{U_2 C_{2u}}{g} \tag{11}$$

As the flow does not precisely follow the blade geometry, the angle of the flow is slightly smaller than the blade's angle. This behavior suggests a quantitative parameter based on the concept of the slip factor that is expressed by Eq. (12) (Gülich, 2010).

$$\sigma = \frac{H_T}{H_{T\infty}} \tag{12}$$

where H_T and $H_{T\infty}$ are the head in the finite and infinite number of blades, respectively. According to Euler's equation, the pump's head is calculated based on the velocity triangle (Eqs. 13 and 14) :

$$H_{T\infty} = \frac{U_2}{g}(U_2 - C_{2m} Cotg\, \beta_{2B}) \tag{13}$$

$$H_T = \frac{U_2}{g}(U_2 - C_{2m} Cotg\, \beta_2) \tag{14}$$

where β_2 and β_{2B} are the actual flow angle and blade angle (flow angle in the state of infinity blade number), respectively.

By considering the relationship between the slip factor and the pump head, the pump head can be improved by modifying the slip factor distribution in the design steps. Therefore, the splitter blades' position alters both the flow direction and slip factor distribution, leading to changes in the head. Numerical simulation can conspicuously assist in appraising the mentioned parameters.

3-5- Surrogate modeling

The metamodeling is evolved from classical design based on the design of experiment (DOE) test design theory, wherein polynomial functions are used either as a response surface or a metamodel. In addition to the commonly used polynomial functions, Sacks et al. (1998) proposed a random model called Kriging.

The relationship between the deterministic computer response and the actual system response is defined in terms of a random function. Neural networks have also been employed for system approximation in response surface production. A combination of polynomial functions and ANNs has also been used in many applications. Although there is no consensus in the literature concerning which model is superior, in recent years, Kriging models have been studied in numerous applications.

Generally, K models are more accurate for nonlinear problems in terms of interpolating the sample points and filtering noise data. Besides, obtaining and using the Kriging models is challenging because they use a global optimization process to identify the most likely answer (R. Jin et al., 2000; G. G. Wang & Shan, 2007). This model is a combination of Gaussian

stochastic processes and polynomial regression. The regression model fits the samples based on least-squares estimation rules. The Kriging formulation is written as Eq. (15):

$$y(x) = f\left(x\right)^T \beta + z(x) \quad (15)$$

Where y(x) is the response function and $f\left(x\right)^T \beta$ is the regression model. In this process, mostly, polynomials up to second-order are used to indicate the global trend of the sample points; f(x) denotes the regression basis function and b shows the regression coefficient; z(x) is the correlation model and is considered an independent Gaussian random process. Detailed information in this regard is available in (Koziel & Leifsson, 2013)

The DOE method has been used in many studies to generate the input/output simulation data in order to fit a Kriging model that utilizes them. Latin Hypercube Sampling (LHS) is a DOE that is applied to cover the entire design range homogeneously. This method generates random sample points considering all represented parts of the design space. The LHS divides each input range into N exclusive and exhaustive distances with equal probability, and samples each input without replacing it (Tolk et al., 2017) .

In this study, 100 samples were extracted using LHS and were used as the inputs of the Kriging response surface model (or Kriging metamodels). In addition to these points, another 30 were produced and set as the test points of the Kriging model. After developing the model, the results of the CFD analysis were extracted for 30 points and compared with the results of the Kriging model. The root means square error (RMSE) between the values estimated by Kriging and the actual values obtained from CFD analysis is calculated using Eq. (16):

$$RMSE = \sqrt{\frac{\sum_i^N d_i^2}{N}} \quad (16)$$

where N is the total number of test points and di is the difference between the estimated values based on Kriging and the values obtained from CFD analysis (di = H (Kriging) - H (CFD)).

The RMSE value calculated based on Eq. (16) is approximately 0.95 and 0.93 for the head and efficiency, respectively, suggesting the acceptable accuracy of the Kriging model. Therefore, the Kriging model can be employed in the optimization process as a surrogate model. In the present study, the splitter blade is parameterized in terms of three characteristics: number (N), length (SL), and peripheral position (α) (Fig. 3).

The length of the splitter (SL) is parameterized as a percentage of the main blade (ML) length, and the peripheral position of the splitters (α) relative to the suction side is parametrized between zero (suction side) to 100% (pressure side) in each channel. The variation range of each parameter is presented in Table 2.

Table 2. Properties of the simulated flows

Splitter parameter	Reference value	Resolution	Range
Blade number (N)	5	Discrete by value	5; 6; 7; 8
Peripheral position (α)	50 %	Continuous	20% - 80%
Length (SL)	55% ML*	Continuous	40% - 75% ML

*ML: Main Blade Length

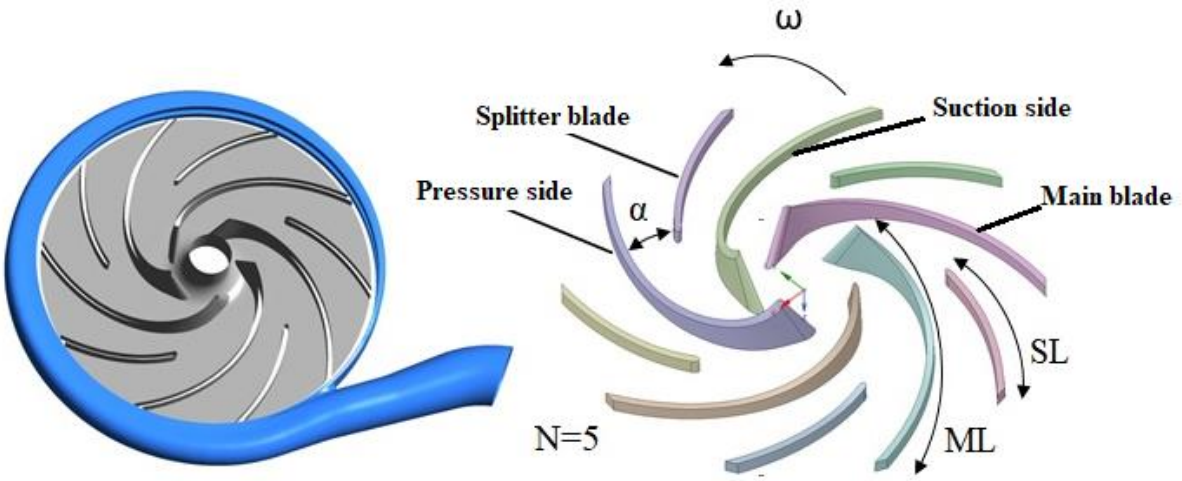

Fig. 3. Splitter design parameters

The number of splitter blades is always equal to the number of main blades. Therefore, according to the initial number of blades (7), this number is selected between 5 and 8. To affect the head and prevent clogging at the inlet section, the length of the splitter blades is determined between 40% and 75% of the main blade's length. Different positions of the splitter blade led to a change in the flow direction through changing the pressure distribution, leading to the change in the velocity distribution in the impeller channel. Therefore, the peripheral position parameter has the most significant impact on the slip factor distribution in the impeller channel. Besides, too much closeness of the splitter to the main blades may block the main channel. Therefore, the range of variation in the peripheral position of splitter blades is from 20% to 80% of the distance between the two main blades.

Table 3 shows a part of the simulation results obtained from the sample points that were used to construct the Kriging model. In this table, the geometric parameters of the splitter, namely N, α, and SL, are the input variables and H and η are the output variables.

Table 3. DOE geometry

Serial no.	Design variables			Objective parameters	
	Blade number	Peripheral position (α) (%)	Splitter length (%ML) (%)	Efficiency (%)	Head (m)
1	8	29.3	49.2	47.4	31.39
2	8	68.3	49.9	48.83	33.16
3	8	73.7	42	48.6	32.32
4	6	41.9	58	51.37	31.52
5	6	58.7	41.1	50.35	30.6
6	7	28.1	44.3	49.31	31.33
7	8	21.5	67.4	46.79	30.26
8	5	77.3	54.7	50.41	29.53
9	6	35.3	40.1	50.94	31.14
10	6	64.1	68.1	50.7	31.36
11	5	62.9	50.8	51.75	29.36
12	8	38.9	62.9	47.46	31.77

3-6- Multi-objective optimization

Multi-objective optimization is used for problems with more than one objective function. These functions may be minimized or maximized simultaneously, or one is minimized and the other is maximized. Therefore, an optimal solution may not be the best for all functions. There is a set of optimal solutions known as Pareto optimal solutions in the domain of multi-objective optimization problems. The curve connecting these optimal points is named the Pareto optimal front.

In the present study, multi-objective optimization was performed using a GA. The Kriging model is utilized to relate variables and objective functions. The combination of RSM and GAs in engineering optimization problems has provided promising results (Siddique et al., 2018; Suh et al., 2019; Wenjie Wang et al., 2017; Y. Zhang et al., 2014).

4- Experimental method

This work concentrates on experimental tests for water and glass-bead slurry at different concentrations. Testbed details and the specifications of measuring instruments are interpreted as follows. The testbed is designed based on ISO 9906 standard (Technical Committee ISO/TC 115 & Technical Committee CEN/TC 197, 2012) for measuring characteristics of pump performance, including discharge, head, and power. The schematic of the designed testbed and the measurement instruments in this study is shown in Fig. 4.

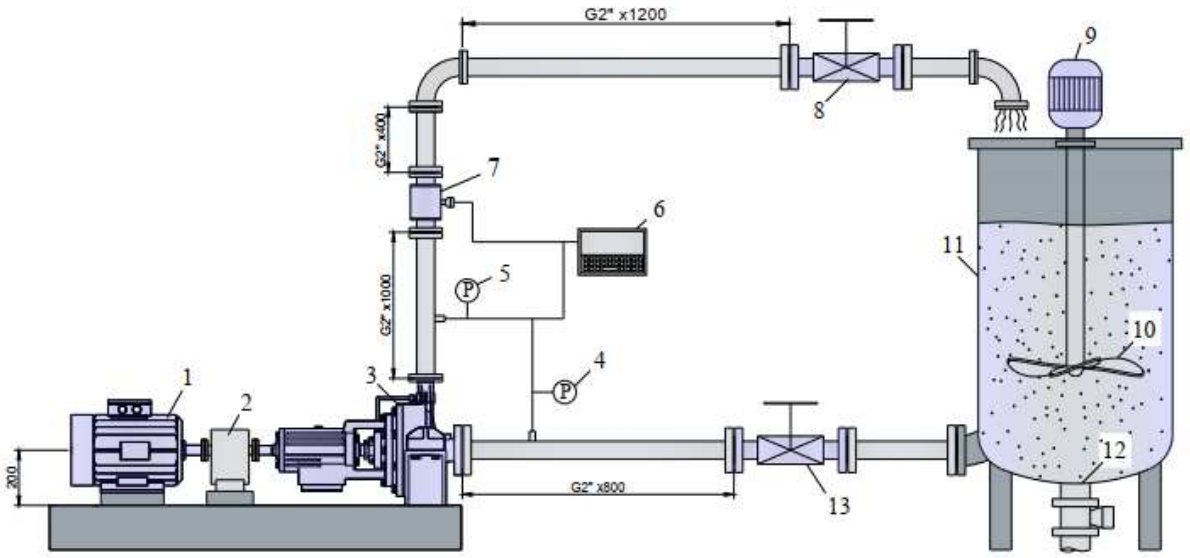

1. Electro Motor
2. Coupling
3. Centrifugal Pump
4. Suction Pressure Transducer
5. Discharge Pressure Transducer
6. Data acquisition System
7. Magnetic Flow Meter
8. Discharge Valve
9. Mixer Motor
10. Mixer
11. Test Tank
12. Drain Valve
13. Suction Valve

Fig. 4. Testbed schematic (all dimensions are in millimeter)

The characteristics of measurement instruments are represented in Table 4. By referring to Table 4, a pressure transducer is used with a vacuum measuring capability of -1.0 bar to +1.0 bar with a precision of ±0.25% full scale (FS) accuracy in the suction side with the output of 4.0-20.0 mA. For the discharge side, a pressure transducer with a measurement range of 0.0-6.0 bar with a precision of ±0.25% FS accuracy is mounted. The flow rate is measured using a 2.0-inch electromagnetic flowmeter with a precision of ±0.2%. The pipes were made of galvanized iron and two valves were used to control the flow rate. These valves were installed at suction and discharge sides. The test tank is a cylindrical type with a diameter of 800.0 mm and a height of 1700.0 mm. A mixer is installed on the tank to maintain the uniformity of the mixture and to prevent sedimentation.

Table 4. Characteristics of measurement instruments

Measurement instrument	Measuring range	Precision (±)	Manufacturer / Model
Suction pressure transmitter	-1.0 to +1.0 bar	0.25 % full scale	Hogller / HOTH
Discharge Pressure transmitter	0.0 to 6.0 bar	0.25 % full scale	Hogller/ HOTH
Flow meter	To 35.0 m3/hr.	0.50 %	Indress+hauser / Promag 53P50
Data acquisition card	15.0 Amperes per line	0.50 %	Advantech / USB 4711

A single-stage horizontal centrifugal pump was selected as the case study with geometric and performance characteristics. The specifications of the pump are presented in Table 5. This pump rotates by a 5.5 kW three-phase squirrel cage motor.
The power consumption of the electromotor is measured using a multi-functional measuring device with a precision of ±0.5% (manufactured by Ziegler, German, and Model: MFM 3430). All measured values of the pump and motor are recorded and stored by a data logger system (See supplementary material S2). The uncertainty of flow rate and head measurements are calculated as 0.5 % and 0.46 %, respectively (Coleman & Steele, 1995) (See supplementary material S3).

Table 5. Characteristics of centrifugal pump case study

Pump type	Capacity (m3/hr)	Head (m)	Speed (rpm)	Impeller dia. (mm)	Impeller width (mm)	Vanes Number	Motor power (kW)
32-160	20.0	30.0	2900.0	169.0	5.0	5	5.5

Fig. 5 shows the impeller geometry of the selected case study (a) and new impeller geometry with a splitter (b).

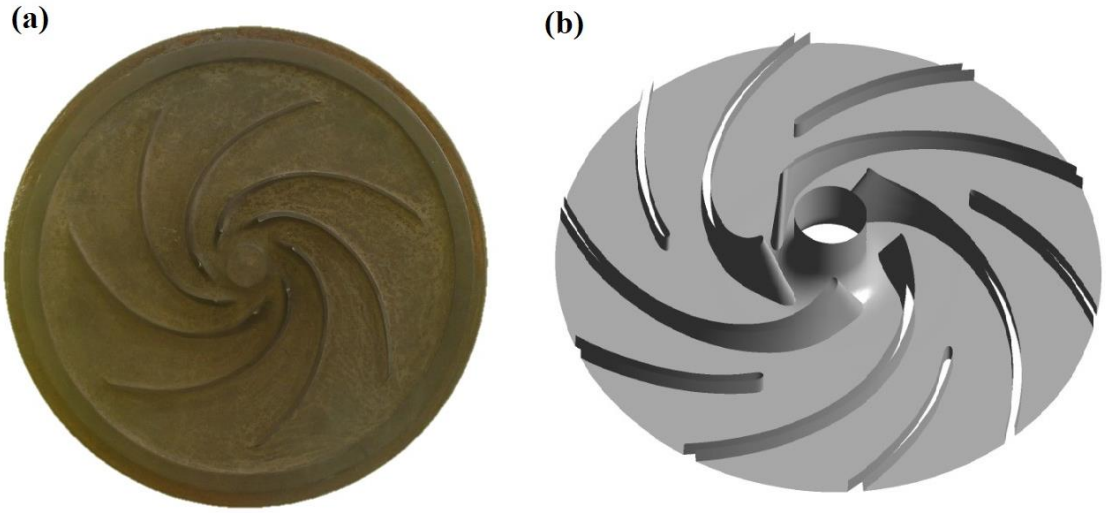

Fig. 5. (a) Impeller geometry of selected case study and (b) new impeller with the splitter

5- Results and discussion

5-1- Comparison of Numerical and Experimental results

The optimization process is based on a numerical simulation and the results of each step. Hence, it is crucial to ensure the accuracy of the simulations and numerical models used. The pump's head-discharge curve obtained from the test and simulation data was used to validate the numerical method and the models. Fig. 6 compares the results of numerical simulation and test at a 5.6% volumetric concentration.

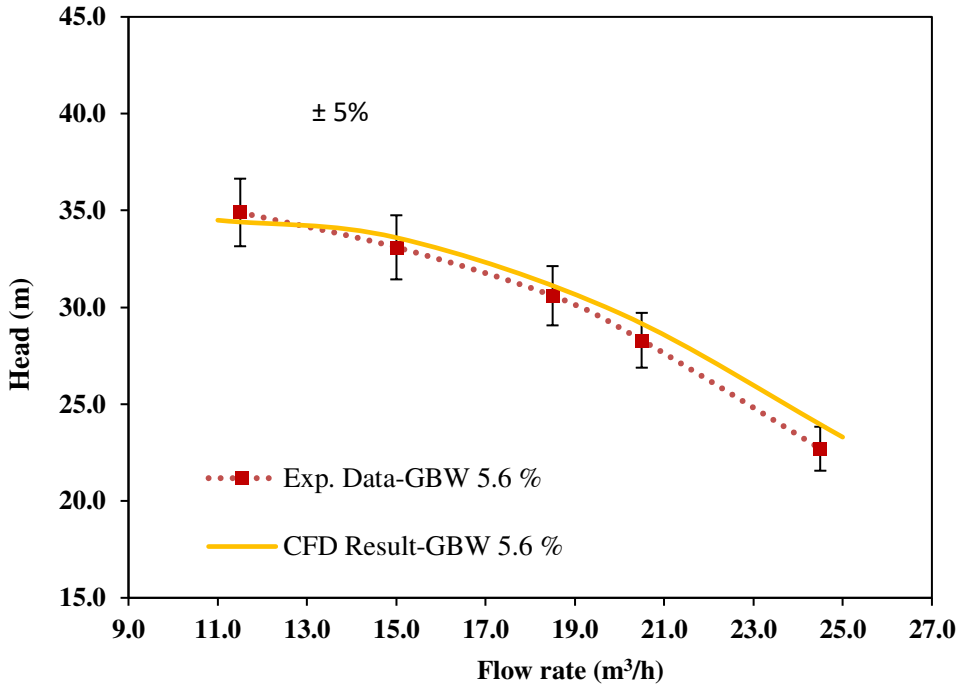

Fig. 6. Comparison of the numerical simulation results (yellow line) with experimental data (red line) for GBW slurry at a concentration of 5.6%

According to Fig. 6, the calculation error is in the ±5% range of the test results, and it increases with the rise in the flow rate. The results show a good correlation between experimental data and numerical solutions with a 0.95 correlation coefficient. Furthermore, the distribution of glass beads in the impeller channel is calculated using a validated numerical solution. The wear-prone locations in the impeller channel can be predicted using particle distribution. As can be seen from Fig. 7, particle accumulation occurs more on the channel pressure side, and thus wear is more likely to occur in this site.

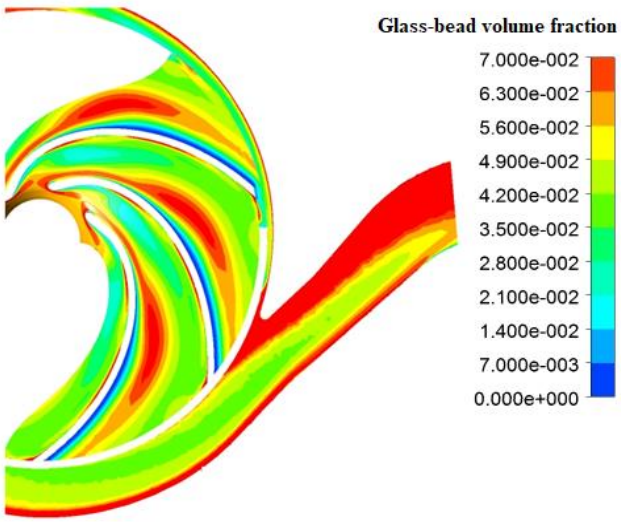

Fig. 7. Distribution of particles volume fraction in the GBW slurry at a concentration of 5.6%

In this study, the slip factor was inaugurated as an effective parameter on the head of centrifugal pumps. Fig. 8 shows the slip factor distribution in the initial impeller channel for a volume fraction of 5.6%. As can be seen, the value of the slip factor decreases by moving from the suction side to the pressure side (0.98 to 0.76), and the flow deviation from the blade increases simultaneously. Due to the lack of blades in the channel's central area (α = 45%), the slip factor shows the lowest amount.

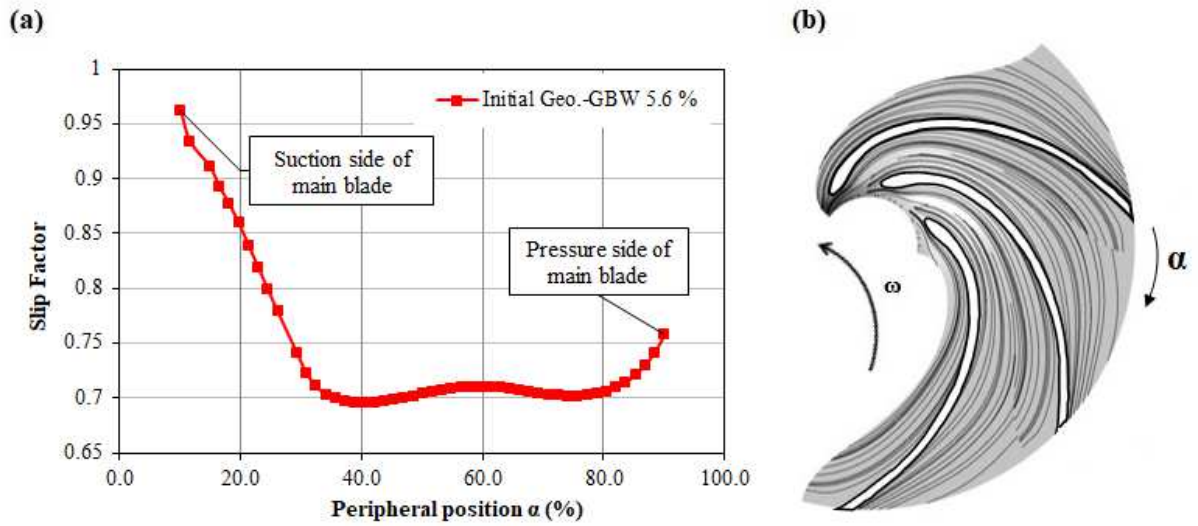

Fig. 8. Distribution of slip factor in the GBW slurry at a concentration of 5.6% in the initial impeller

To comprehend the effect of particles on the slip factor distribution in detail, the average slip factor in the direction of the blade height from the hub to the shroud section is calculated based on numerical results. Fig. 9 compares the slip factor distribution in water and glass bead slurry, with volume fractions of 5.6% and 10%. According to these results, the average slip factor from the hub to the shroud decreases in the span range of 0 to 45 and then undergoes a rise from this range to the span of 100. In other words, the factor is close to 1 in the close vicinity of a wall and has its lowest value at the span of 50%.

The difference between results is due to the presence of walls near the hub and shroud section and, as well as the absence of the wall in a 50% span. Also, Fig. 9 confirms that by increasing particle volume fraction, the slip factor decreases more distinctively.

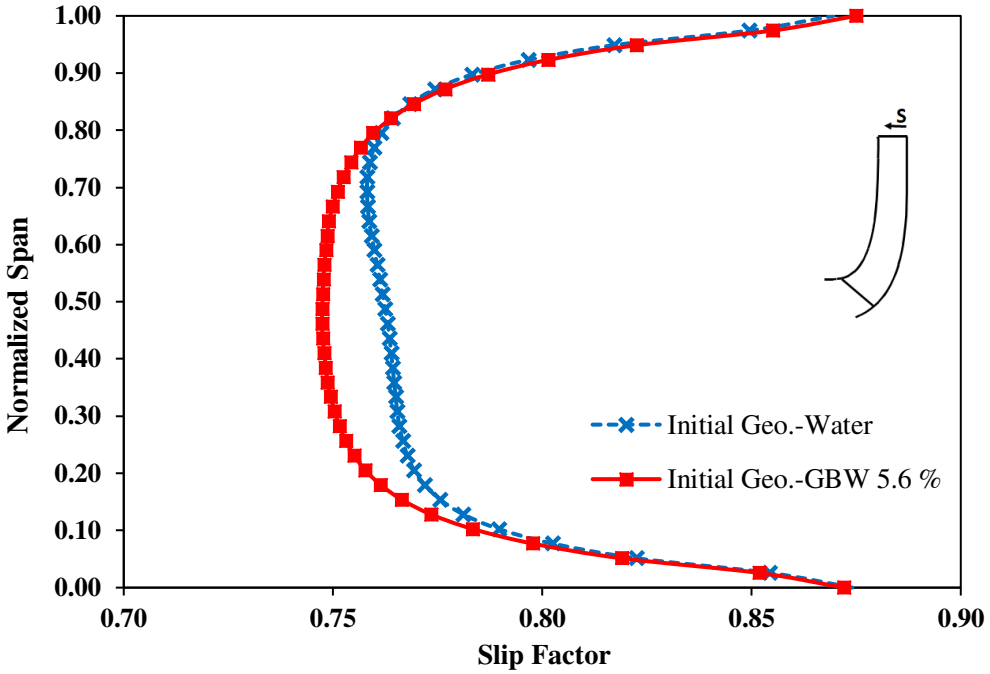

Fig. 9. Comparison of the slip factor in the blade height direction from hub to shroud for water and GBW 5.6% slurry

Therefore, it can be concluded that slurry flow increases wear and decrease pump life while reducing slip factor (reducing head). To achieve optimal geometry, the analysis presented in the comparative Figs. 8 and 9 cannot be efficient in determining the characteristics and location of splitter blades. Accordingly, determining the optimal geometry of splitter blades requires a multi-objective optimization process in such a way that the head is maximized and thus, the efficiency does not decline significantly.

5-2- Finding the optimum splitter blade

To execute the optimization process accurately, first, the sensitivity analysis of the output parameters in terms of input variables is performed using the constructed Kriging model (see section 3.5). In this approach, the sensitivity of head and efficiency as output parameters is evaluated in terms of the three input variables such as number, length, and peripheral position of the splitter blades.

Fig. 10 illustrates the head's sensitivity to blade number and peripheral position in a three-dimensional diagram.

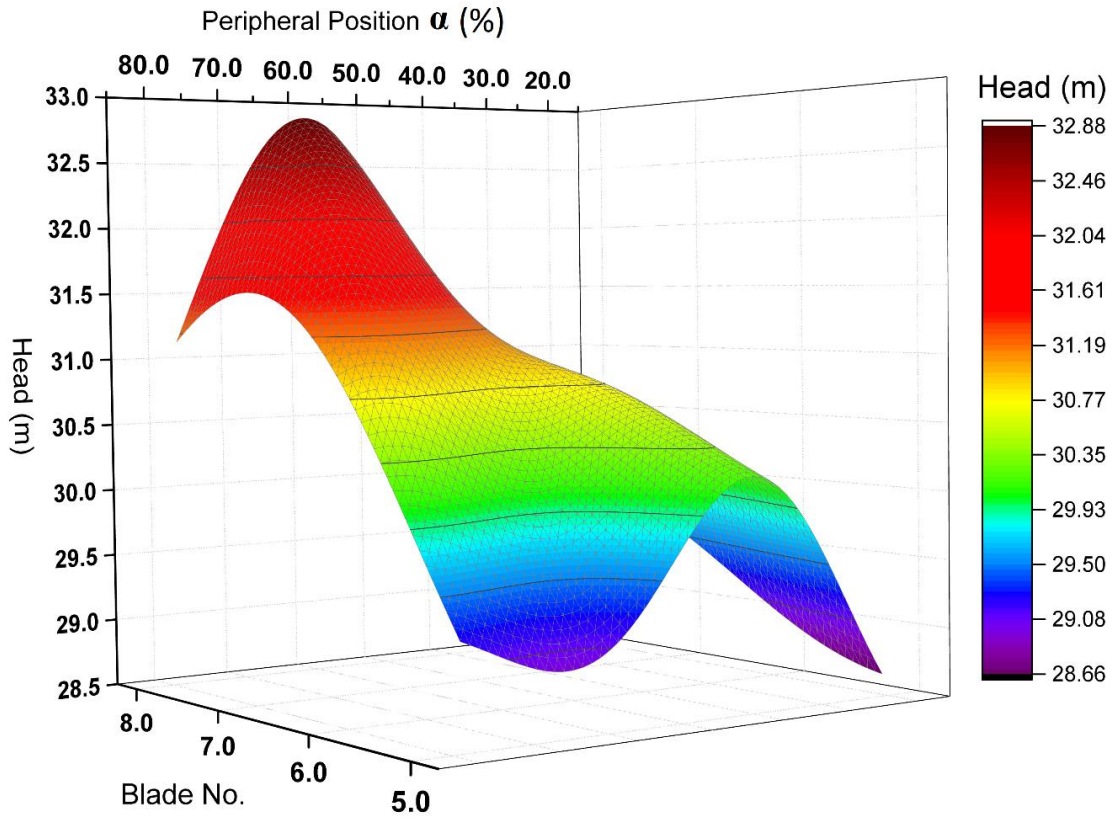

Fig. 10. Effect of splitter blade number and peripheral position on the head

Accordingly, it is found that as the number of blades increases from 5 to 8, the head increases from 29.2 m to 32.9 m. Also, moving the splitter toward the pressure side (α > 50%), the head increases. Fig. 11 is used to explain the sensitivity of the pump efficiency to the two parameters blade number and peripheral position for integrated analysis and compared with Fig. 10. According to Fig. 11, by increasing the number of blades from 5 to 8, the efficiency has a Gaussian distribution curve changing in the range of 49.7% to 46.6%, and its maximum point corresponds to 6 numbers of blades. Moreover, the head increases by moving the splitter toward the pressure side (α > 50%).

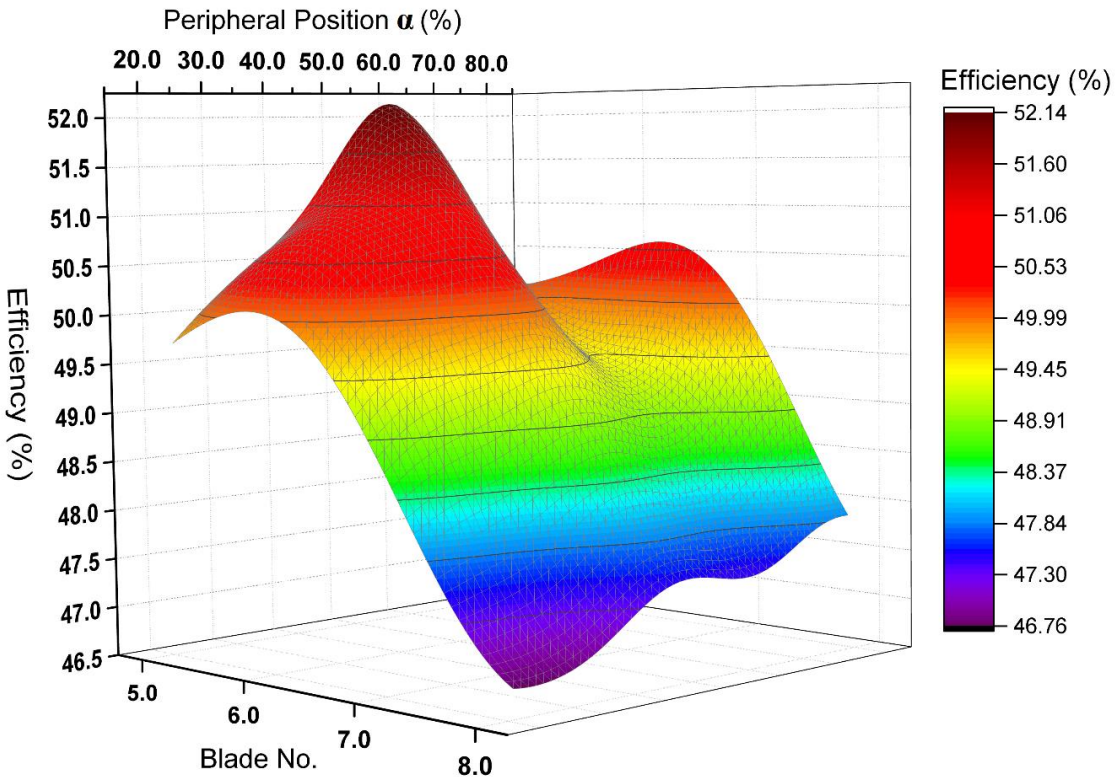

Fig. 11. Effect of splitter blade number and peripheral position on efficiency

Fig. 12 presents the effect of the splitter peripheral position on the head in a two-dimensional curve. According to this figure, as the splitter moves toward α > 50%, first the head increases and then decreases. In addition, head values at α > 50% are higher than those at α < 50%, suggesting the greater effect of the splitter blades on increasing the pump head when the splitters are at α > 50%.

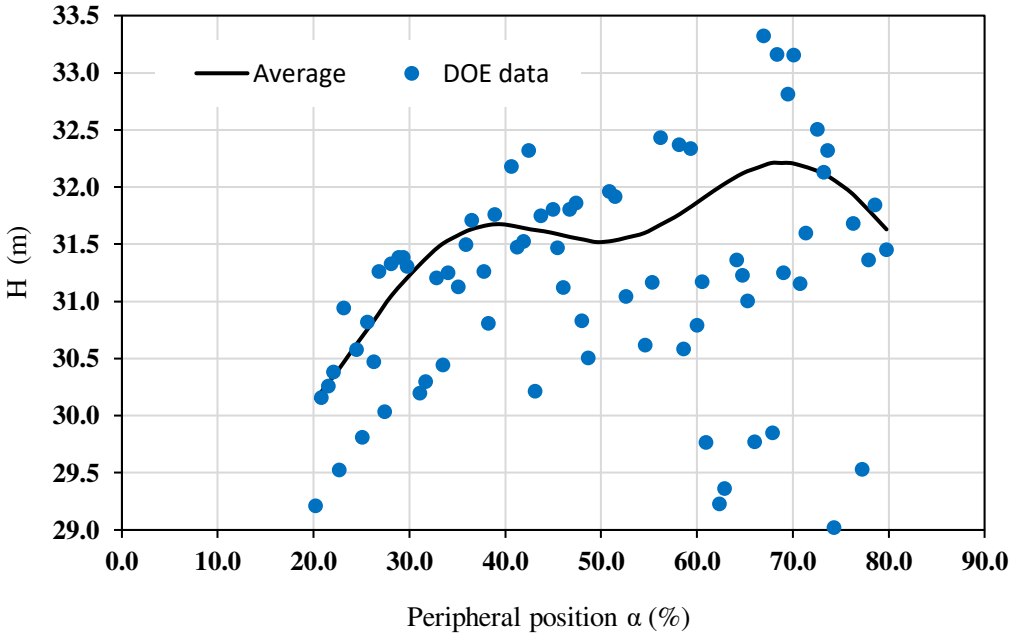

Fig. 12. Effect of splitter blade position on the head

Therefore, achieving the splitter optimal geometry considering the influence of the head and efficiency interactions (Figs. 10, 11, and 12) requires an optimization process.
According to the explanations provided in section 3.6, the optimization process was performed by combining experimental design techniques, RSMs, and GAs. Table 6 presents the values of three influential parameters in determining the optimal shape and position of splitter blades using the optimization model.

Table 6. Primary and optimized parameter of the splitter

Splitter parameter	Reference value	Optimized value
Blade number (N)	5	6
Peripheral position (α)	50 %	67.2%
Length (SL)	55% ML	62.8% ML

A comparison of primary and optimized geometry in the optimization process is provided in Fig. 13.

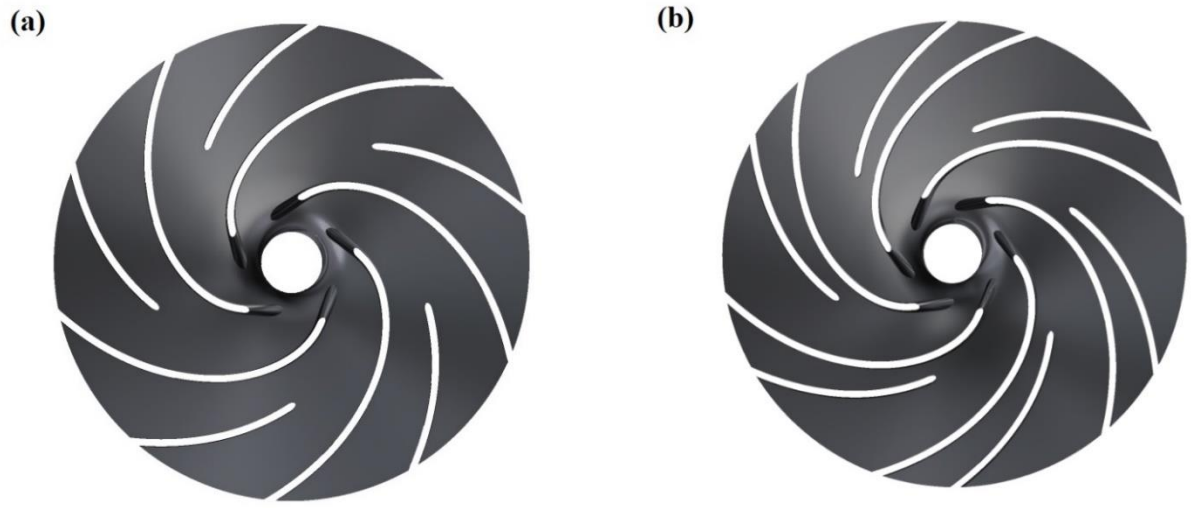

Fig. 13. Comparison of primary (a) and optimal geometry (b) of the impeller in the optimization process

5-3- Hydrodynamic performance of the optimum slurry pump

The simulation of the initial (Fig. 5(a)) and optimized geometry (Fig. 13(b)) in slurry flow with a concentration of 5.6% was performed using a two-phase ASM model to evaluate the optimization results. Fig. 14 shows the comparison of head and efficiency values in the two initial and optimal models. From Fig. 14, it can be inferred that the goal of optimization (i.e., increasing the head and maintaining the efficiency in the range of initial values) is well met. Thus, the head is increased between 5% and 6% compared to the initial model and the efficiency remains in the initial value range with a variation of less than 1.5% (Fig. 14).
According to Fig. 14, a good correlation based on the exponential model exists in the head-discharge curve between the initial model and the optimized one (R2 = 0.96). Moreover, there is a similar trend for the efficiency-discharge curve of both models (R2 = 0.95). According to

Fig. 14, the best efficiency point (BEP) of the initial model is 19 m^3/h, while it is 18 m^3/h for the optimal model. Therefore, it can be concluded that the BEP of the optimal model has moved toward lower flow rates than the initial model (from 19 m3/h to 18 m3/h). This result is attributed to the addition of splitter blades and consequently clogging of the impeller channel in the new geometry.

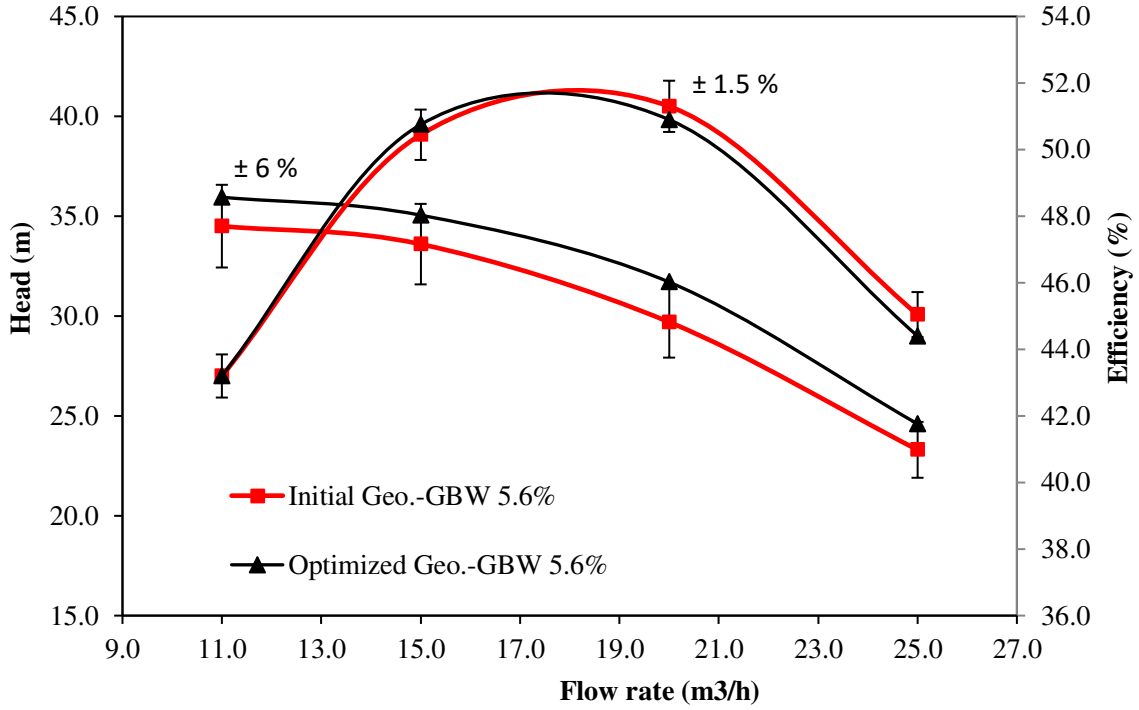

Fig. 14. Comparison of head and efficiency in the initial and optimized impeller

Fig. 15 shows the distribution of glass beads in the optimized impeller channel at a concentration of 5.6% to complete the analysis above.

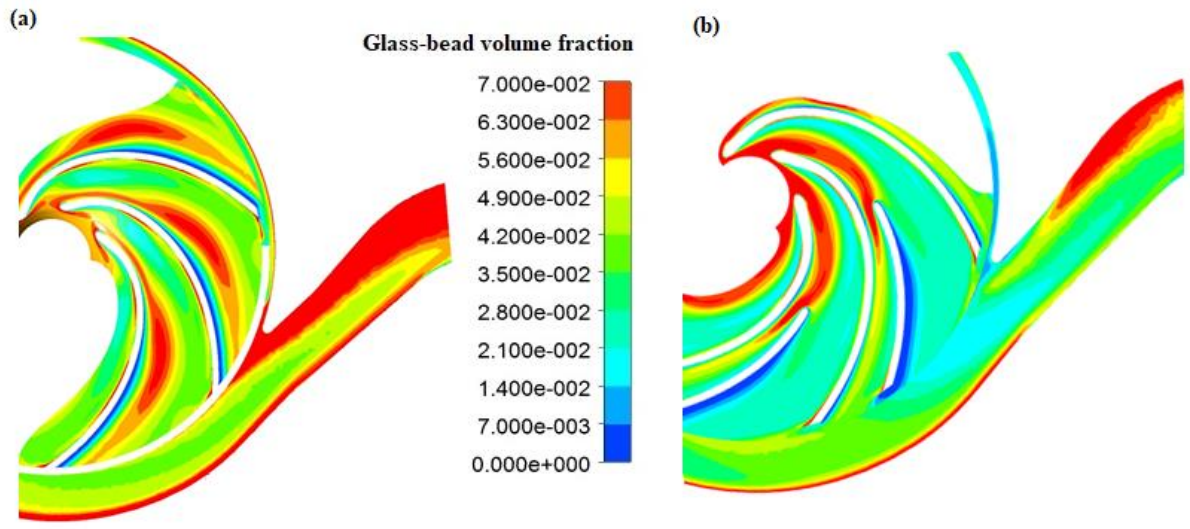

Fig. 15. Comparison of solid distribution in the initial and optimized impeller

Fig. 15 shows a more uniform distribution of particles in a large part of the optimized impeller channel. As can be seen, due to the addition of splitter blades and the reduction of the flow passage in the optimized geometry, the accumulation of particles in the impeller inlet of the optimized geometry is higher compared to the initial geometry.

Fig. 16 shows how the slip factor changes through the impeller channel between the two main blades for the initial and optimal impeller. In this figure, the continuous and discrete curve corresponds to the initial impeller and optimal impeller, respectively. The discontinuity point in the optimal impeller diagram pertains to the splitter blades. In general, both before and after the splitter, the slip factor decreases from the pressure side to the suction nuzzle in both parts of the impeller channel.

Also, compared to the initial values, the amount of slip factor has increased in the whole area. This figure demonstrates that the addition of splitter blades improves the pump slip factor and thus increases the pump head.

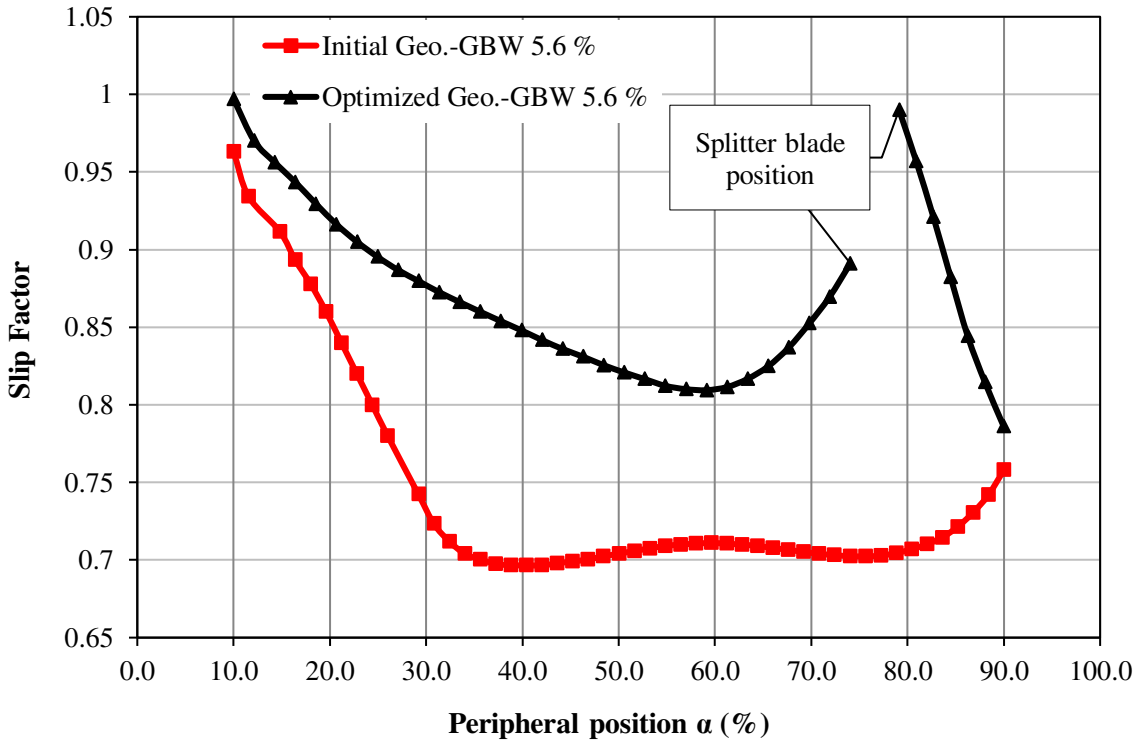

Fig. 16. Peripheral distribution of slip factor in the optimized impeller channel

To investigate the general effect of adding splitter blades on the slip factor, the change curve of the mean slip factor in the blade height direction from the hub to the shroud is drawn in Fig. 17.

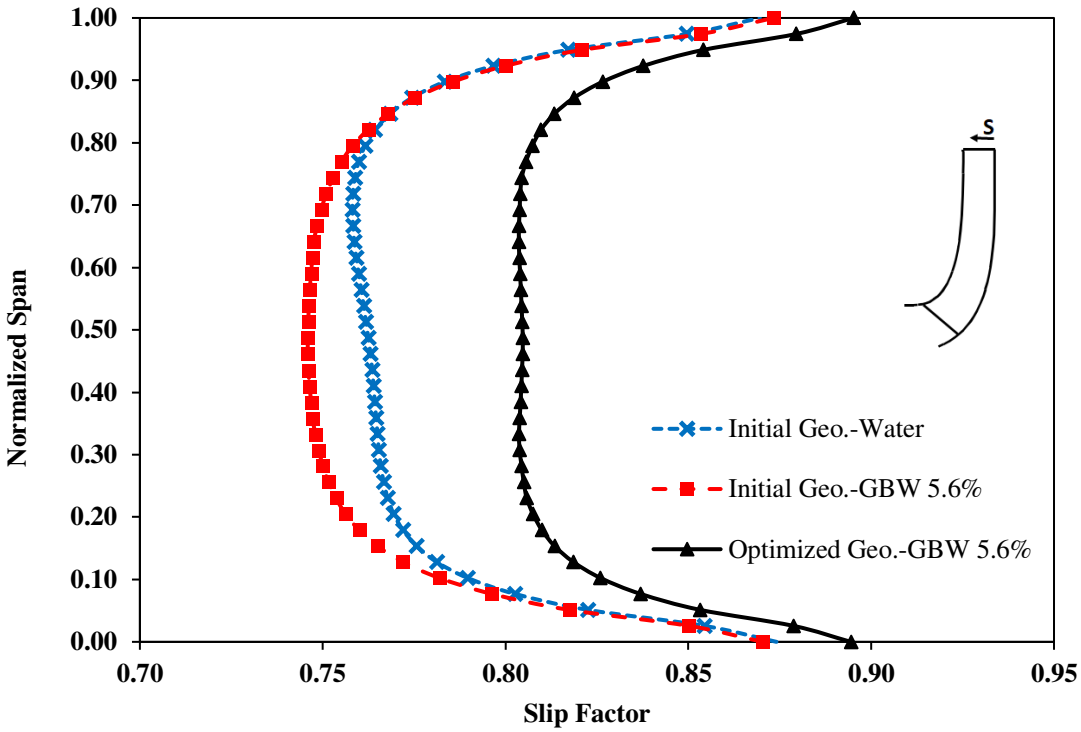

Fig. 17. Height distribution of slip factor in optimized impeller from hub to shroud

Fig. 17 shows that the slip factor has increased in all sections between the hub and the shroud compared to the initial impeller. In the optimal case, the amount of slip factor at 50% of the impeller span is approximately 7% more than the initial value. Also, a more uniform distribution of the slip factor is visible in the middle of the channel.

6- Conclusion

The slip factor is an effective design parameter in centrifugal pump head values that varies by the geometry and flow parameters. This study focuses on the effect of adding splitter blades on slip factor and centrifugal pump head. A pump was selected as the case study and the numerical analysis method was performed using a two-phase ASM model. The numerical method was validated based on experimental tests for water and slurry. According to the acquired results, the particle accumulation on the pressure side of the impeller channel is higher, and the slip factor in these locations reduces in a greater range. Also, the accumulation of particles at this location can undoubtedly increase wear in this region. One way to improve the slip factor and head in a centrifugal pump is to add splitter blades in optimal locations. The optimization process was performed using a combination of experimental design techniques, response surface surrogate methods, and GA to determine the best position to add splitter blades and determine their optimal geometric characteristics. According to the results, the optimal impeller has one blade less than the initial model and has 6 main blades and 6 splitters. The optimal location of the splitter is in 67.2% of the distance between two main blades and close to the pressure side. Besides, the optimal length of the splitter blades is 62.8% of the length of the main blades. The addition of splitters also improved the head by 6.7%, and the efficiency remained reasonably constant at the initial values. Accordingly, reducing the number of blades and adding splitters not only improve pump performance and increase the head but also reduce

wear head due to the reduction in the number of the main blades and opening of the impeller inlet. As a result, pump life will increase as well. The results of this study can assist designers of slurry pumps to determine the optimal position of adding splitter blades.

Declarations:

Availability of data and materials

All data generated or analyzed during this study are included in this published article.

Competing interests

The authors declare that they have no competing interests.

Funding

There is no funding for this article.

Authors' contributions

Ehsan Abdolahnejad, Mahdi Moghimi, Shahram Derakhshan

E.A.; Designed and performed experiments, performed the numerical simulations, performed the optimization process and co-wrote the paper. M.M.; Designed experiments, analyzed data and co-wrote the paper. S.D.; Supervised the research and co-wrote the paper.

Acknowledgments

The authors gratefully acknowledge the support of Berkeh pumps Company and Mr. Masoud Reza Soltani in this study.

References:

Bandler, J. W., Cheng, Q. S., Dakroury, S. A., Mohamed, A. S., Bakr, M. H., Madsen, K., & Søndergaard, J. (2004). Space mapping: The state of the art. *IEEE Transactions on Microwave Theory and Techniques*, *52*(1 II), 337–361. https://doi.org/10.1109/TMTT.2003.820904

Caridad, J., & Kenyery, F. (2004). CFD Analysis of Electric Submersible Pumps (ESP) Handling Two-Phase Mixtures. *Journal of Energy Resources Technology*, *126*(2), 99. https://doi.org/10.1115/1.1725156

Cavazzini, G., Pavesi, G., Santolin, A., Ardizzon, G., & Lorenzi, R. (2015). Using splitter blades to improve suction performance of centrifugal impeller pumps. *Proceedings of the Institution of Mechanical Engineers, Part A: Journal of Power and Energy*, *229*(3), 309–323. https://doi.org/10.1177/0957650914563364

Coleman, H. W., & Steele, W. G. (1995). Engineering application of experimental uncertainty analysis. *AIAA Journal*, *33*(10), 1888–1896. https://doi.org/http://dx.doi.org/10.2514/3.12742

Crowe, clayton T., Schwarzkopf, J. D., Sommerfeld, M., & Tsuji, Y. (2012). *Multiphase flows with droplets and particles*. CRC Press. http://www.crcpress.com

Derakhshan, S., Mohammadi, B., & Nourbakhsh, A. (2008). Incomplete sensitivities for 3D radial turbomachinery blade optimization. *Computers and Fluids*, *37*(10), 1354–1363. https://doi.org/10.1016/j.compfluid.2008.01.002

Derakhshan, S., Mohammadi, B., & Nourbakhsh, A. (2009). Efficiency Improvement of Centrifugal Reverse Pumps. *Journal of Fluids Engineering*, *131*(2), 021103. https://doi.org/10.1115/1.3059700

Derakhshan, S., Mohammadi, B., & Nourbakhsh, A. (2010). The comparison of incomplete sensitivities and Genetic algorithms applications in 3D radial turbomachinery blade optimization. *Computers and Fluids*, *39*(10), 2022–2029. https://doi.org/10.1016/j.compfluid.2010.07.003

Derakhshan, S., Pourmahdavi, M., Abdolahnejad, E., Reihani, A., & Ojaghi, A. (2013). Numerical shape optimization of a centrifugal pump impeller using artificial bee colony algorithm. *Computers & Fluids*, *81*, 145–151. https://doi.org/10.1016/j.compfluid.2013.04.018

Gölcü, M. (2006). Artificial neural network based modeling of performance characteristics of deep well pumps with splitter blade. *Energy Conversion and Management*, *47*(18–19),

3333–3343. https://doi.org/10.1016/j.enconman.2006.01.011

Gui, L., Gu, C., & Chang, H. (1989). Influences of splitter blades on the Centrifugal fan performances. *Proceedings of the ASME Turbo Expo*, *1*(1984). https://doi.org/10.1115/89GT-33

Gülich, J. F. (2010). Centrifugal Pumps. In Intergovernmental Panel on Climate Change (Ed.), *Antimicrobial agents and chemotherapy* (Vol. 58, Issue 12). Springer Berlin Heidelberg. https://doi.org/10.1007/978-3-642-12824-0

Haslinger, J., & Mäkinen, R. A. E. (2003). *Introduction to shape optimization : theory, approximation, and computation*. SIAM, Society for Industrial and Applied Mathematics.

Heo, M.-W., Kim, J.-H., & Kim, K.-Y. (2015). Design Optimization of a Centrifugal Fan with Splitter Blades. *International Journal of Turbo & Jet-Engines*, *32*(2), 143–154. https://doi.org/10.1515/tjj-2014-0026

Hirt, C. ., & Nichols, B. . (1981). Volume of fluid (VOF) method for the dynamics of free doundaries. *Journal of Computational Physics*, *39*, 201–225. https://doi.org/10.1007/s40998-018-0069-1

Hydraulic Institute, Europump, & Office of Industrial Technologies - US Department of Energy. (2001). Pump Life Cycle Costs: A Guide to LCC Analysis for Pumping Systems - Executive Summary. In *Renewable Energy*.

Ishii, M. (1975). *Thermo-fluid dynamic theory of two-phase flow*. https://inis.iaea.org/search/search.aspx?orig_q=RN:7233706

Jin, R., Chen, W., & Simpson, T. W. (2000). Comparative studies of metamodeling techniques under multiple modeling criteria. *8th Symposium on Multidisciplinary Analysis and Optimization*, *c*. https://doi.org/10.2514/6.2000-4801

Jin, Y. (2011). Surrogate-assisted evolutionary computation: Recent advances and future challenges. *Swarm and Evolutionary Computation*, *1*(2), 61–70. https://doi.org/10.1016/j.swevo.2011.05.001

Kergourlay, G., Younsi, M., Bakir, F., & Rey, R. (2007). Influence of splitter blades on the flow field of a centrifugal pump: Test-analysis comparison. *International Journal of Rotating Machinery*, *2007*. https://doi.org/10.1155/2007/85024

Khoeini, D., & Tavakoli, M. R. (2018). The optimum position of impeller splitter blades of a centrifugal pump equipped with vaned diffuser. *FME Transactions*, *46*(2), 205–210. https://doi.org/10.5937/fmet1802205K

Kleijnen, J. P. C. (2009). Kriging metamodeling in simulation: A review. *European Journal*

of Operational Research, *192*(3), 707–716. https://doi.org/10.1016/j.ejor.2007.10.013

Korkmaz, E., Gölcü, M., & Kurbanoğlu, C. (2017). Effects of blade discharge angle, blade number and splitter blade length on deep well pump performance. *Journal of Applied Fluid Mechanics*, *10*(2), 529–540. https://doi.org/10.18869/acadpub.jafm.73.239.26056

Koziel, S., & Leifsson, L. (2013). *Surrogate-Based Modeling and Optimization*. Springer Berlin Heidelberg.

Li, G., Wang, Y., Cao, P., Zhang, J., & Mao, J. (2018). Effects of the Splitter Blade on the Performance of a Pump-Turbine in Pump Mode. *Mathematical Problems in Engineering*, *2018*. https://doi.org/10.1155/2018/2403179

Lu, Y. M., Wang, X. F., Wang, W., & Zhou, F. M. (2018). Application of the Modified Inverse Design Method in the Optimization of the Runner Blade of a Mixed-Flow Pump. *Chinese Journal of Mechanical Engineering (English Edition)*, *31*(1). https://doi.org/10.1186/s10033-018-0302-x

Manninen, M., & Taivassalo, V. (1996). On the mixture model for multiphase flow. *VTT Publications*, *288*, 3–67.

Martin, J. D. (2009). Computational improvements to estimating Kriging metamodel parameters. *Journal of Mechanical Design, Transactions of the ASME*, *131*(8), 0845011–0845017. https://doi.org/10.1115/1.3151807

Miyamoto, H., Nakashima, Y., & Ohba, H. (1992). Effects of splitter blade op the flows and characteristics in centrifugal impellers. *JSME International Journal*, *35*(2), 238–246. http://www.mendeley.com/research/geology-volcanic-history-eruptive-style-yakedake-volcano-group-central-japan/

Nabil, T., El-Sawaf, I., & El-Nahhas, K. (2013). Computational fluid dynamics simulation of the solid-liquid slurry flow in a pipeline. *17th International Water Technologies …*, *November*, 5–7. http://iwtc.info/wp-content/uploads/2013/11/137.pdf

Namazizadeh, M., Gevari, M. T., Mojaddam, M., & Vajdi, M. (2020). Optimization of the Splitter Blade Configuration and Geometry of a Centrifugal Pump Impeller using Design of Experiment. *Journal of Applied Fluid Mechanics*, *13*(1), 89–101. https://doi.org/10.29252/jafm.13.01.29856

Nourbakhsh, A., Safikhani, H., & Derakhshan, S. (2011). The comparison of multi-objective particle swarm optimization and NSGA II algorithm: applications in centrifugal pumps. *Engineering Optimization*, *43*(10), 1095–1113. https://doi.org/10.1080/0305215X.2010.542811

Ofei, T. N., & Ismail, A. Y. (2016). *Eulerian-Eulerian Simulation of Particle-Liquid Slurry*

Flow in Horizontal Pipe. *2016*.

Pei, J., Wang, W., & Yuan, S. (2016). Multi-point optimization on meridional shape of a centrifugal pump impeller for performance improvement. *Journal of Mechanical Science and Technology*, *30*(11), 4949–4960. https://doi.org/10.1007/s12206-016-1015-7

Pei, J., Yin, T., Yuan, S., Wang, W., & Wang, J. (2017). Cavitation optimization for a centrifugal pump impeller by using orthogonal design of experiment. *Chinese Journal of Mechanical Engineering (English Edition)*, *30*(1), 103–109. https://doi.org/10.3901/CJME.2016.1024.125

Pericleous, K. A., & Drake, S. N. (1986). An Algebraic Slip Model of PHOENICS for Multi-phase Applications. *Numerical Simulation of Fluid Flow and Heat/Mass Transfer Processes*, *18*, 375–385.

Sacks, J., Welch, W., Mitchell, T., & Wynn, H. (1998). Design and analysis of computer experiments. *Statistical Science*, *4*(4), 409–423. https://doi.org/10.1214/ss/1177012420

Schiller, L., & Naumann, A. (1935). A drag coefficient correlation. *Zeitschrift Des Vereins Deutscher Ingenieure*, *77*, 318–320.

Siddique, M. H., Afzal, A., & Samad, A. (2018). Design Optimization of the Centrifugal Pumps via Low Fidelity Models. *Mathematical Problems in Engineering*, *2018*. https://doi.org/10.1155/2018/3987594

Suh, J. W., Kim, J. W., Choi, Y. S., Kim, J. H., Joo, W. G., & Lee, K. Y. (2018). Development of numerical Eulerian-Eulerian models for simulating multiphase pumps. *Journal of Petroleum Science and Engineering*, 588–601. https://doi.org/10.1016/j.petrol.2017.10.073

Suh, J. W., Yang, H. M., Kim, Y. I., Lee, K. Y., Kim, J. H., Joo, W. G., & Choi, Y. S. (2019). Multi-objective optimization of a high efficiency and suction performance for mixed-flow pump impeller. *Engineering Applications of Computational Fluid Mechanics*, *13*(1), 744–762. https://doi.org/10.1080/19942060.2019.1643408

Technical Committee ISO/TC 115, P., & Technical Committee CEN/TC 197, P. (2012). Rotodynamic pumps — Hydraulic performance acceptance tests — Grades 1 and 2 (BS EN ISO 9906:2012). *International Organisation for Standardisation*, *3*, 59. http://www.iso.org/iso/iso_catalogue/catalogue_tc/catalogue_detail.htm?csnumber=41202

Tolk, A., Fowler, J., & Shao, G. (2017). *Advances in Modeling and Simulation*. https://doi.org/10.1007/978-3-319-64182-9

Torre, F., Konno, S., Lettieri, C., Pini, M., & Kawata, Y. (2018). Design optimization of splitter blades for rocket engine turbopump. *Proceedings of the ASME Turbo Expo*, *2*D-*2018*, 1–11. https://doi.org/10.1115/GT201875192

Wang, G. G., & Shan, S. (2007). Review of metamodeling techniques in support of engineering design optimization. *Journal of Mechanical Design, Transactions of the ASME*, *129*(4), 370–380. https://doi.org/10.1115/1.2429697

Wang, W, Pei, J., Yuan, S., Zhang, J., Yuan, J., & Xu, C. (2016). Application of Different Surrogate Models on the Optimization of Centrifugal Pump. *Journal of Mechanical Science and Technology*, *30*(2), 567–574. https://doi.org/10.1007/s12206-016-0110-0

Wang, Wenjie, Osman, M. K., Pei, J., Gan, X., & Yin, T. (2019). Artificial neural networks approach for a multi-objective cavitation optimization design in a double-suction centrifugal pump. *Processes*, *7*(5), 1–24. https://doi.org/10.3390/pr7050246

Wang, Wenjie, Yuan, S., Pei, J., & Zhang, J. (2017). Optimization of the diffuser in a centrifugal pump by combining response surface method with multi-island genetic algorithm. *Proceedings of the Institution of Mechanical Engineers, Part E: Journal of Process Mechanical Engineering*, *231*(2), 191–201. https://doi.org/10.1177/0954408915586310

Wu, B., Wang, X., Liu, H., & Xu, H. (2015). Numerical simulation and analysis of solid-liquid two-phase three-dimensional unsteady flow in centrifugal slurry pump. *Journal of Central South University*, *22*(8), 3008–3016. https://doi.org/10.1007/s11771-015-2837-7

Yuan, Y., & Yuan, S. (2017). Analyzing the effects of splitter blade on the performance characteristics for a high-speed centrifugal pump. *Advances in Mechanical Engineering*, *9*(12), 1–11. https://doi.org/10.1177/1687814017745251

Zhang, J., Li, G., Mao, J., Yuan, S., Qu, Y., & Jia, J. (2018). Effects of the outlet position of splitter blade on the flow characteristics in low-specific-speed centrifugal pump. *Advances in Mechanical Engineering*, *10*(7), 1–12. https://doi.org/10.1177/1687814018789525

Zhang, Y., Hu, S., Wu, J., Zhang, Y., & Chen, L. (2014). Multi-objective optimization of double suction centrifugal pump using Kriging metamodels. *Advances in Engineering Software*, *74*, 16–26. https://doi.org/10.1016/j.advengsoft.2014.04.001

Zheng, Y., Hu, S., Wu, J., Zhang, Y., & Chen, L. (2014). Multi-objective optimization of double suction centrifugal pump using Kriging metamodels. *Advances in Engineering Software*, *74*, 16–26. https://doi.org/10.1016/j.advengsoft.2014.04.001

Figures

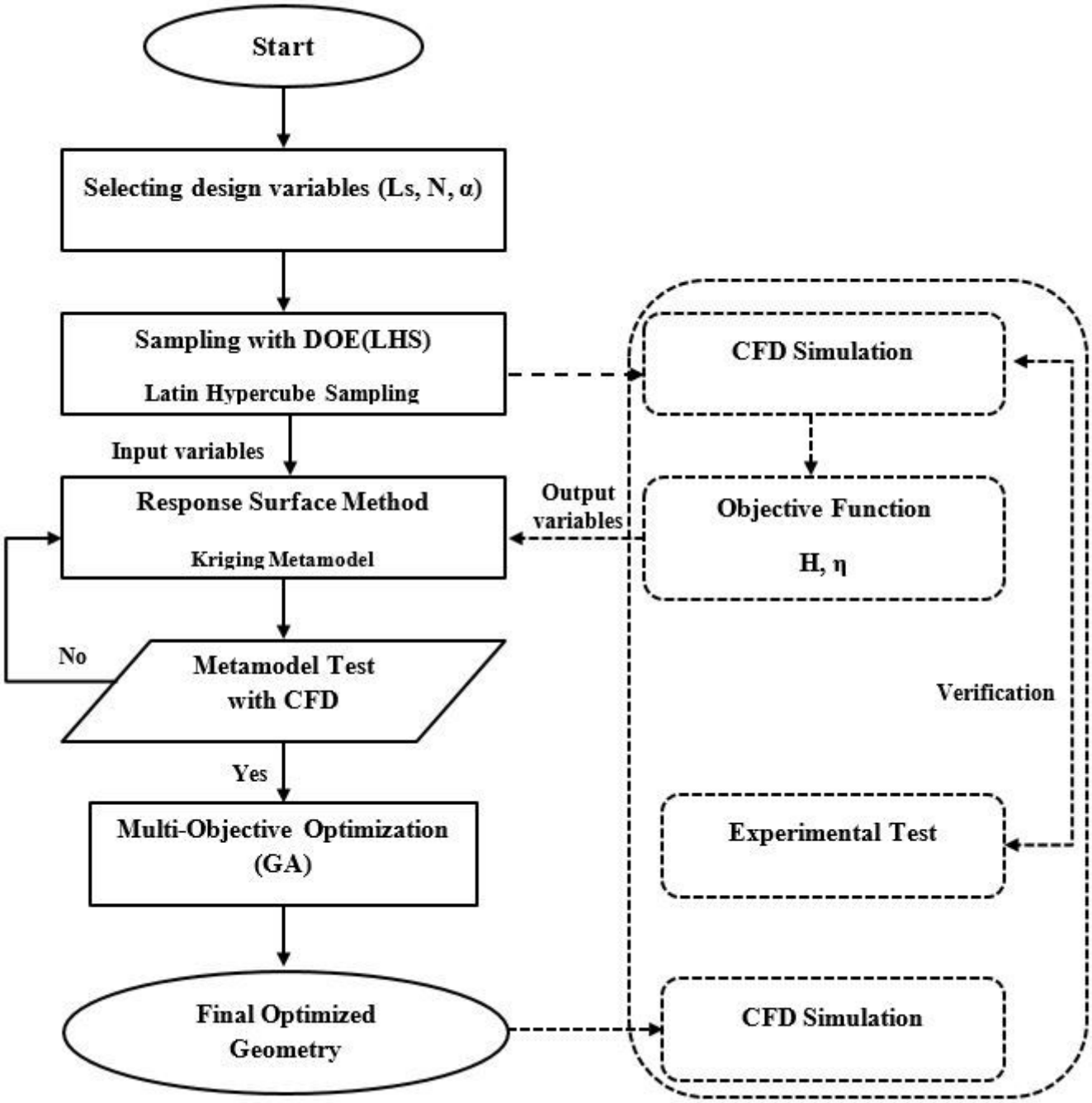

Figure 1

Flow diagram of the optimization

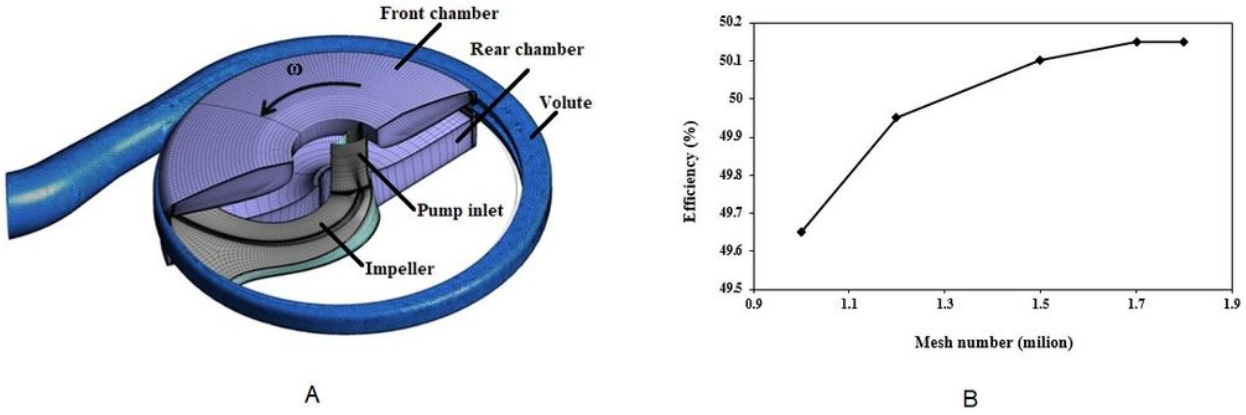

Figure 2

(a). Final generated mesh for the complete computational domain (b). Mesh independency for the complete computational domain

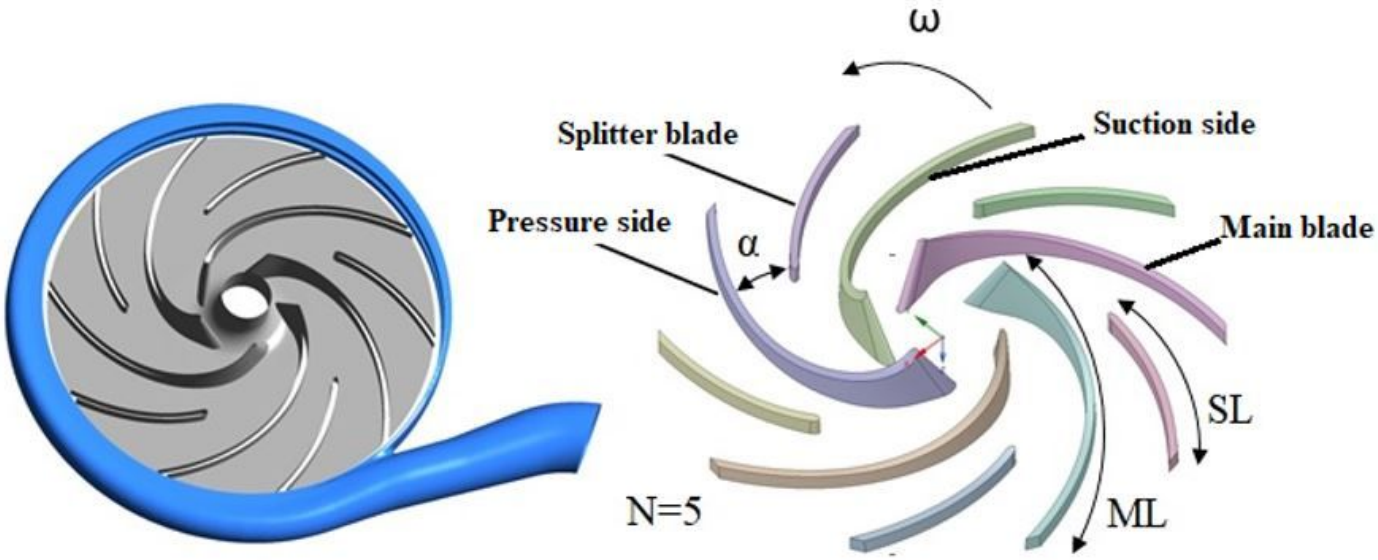

Figure 3

Splitter design parameters

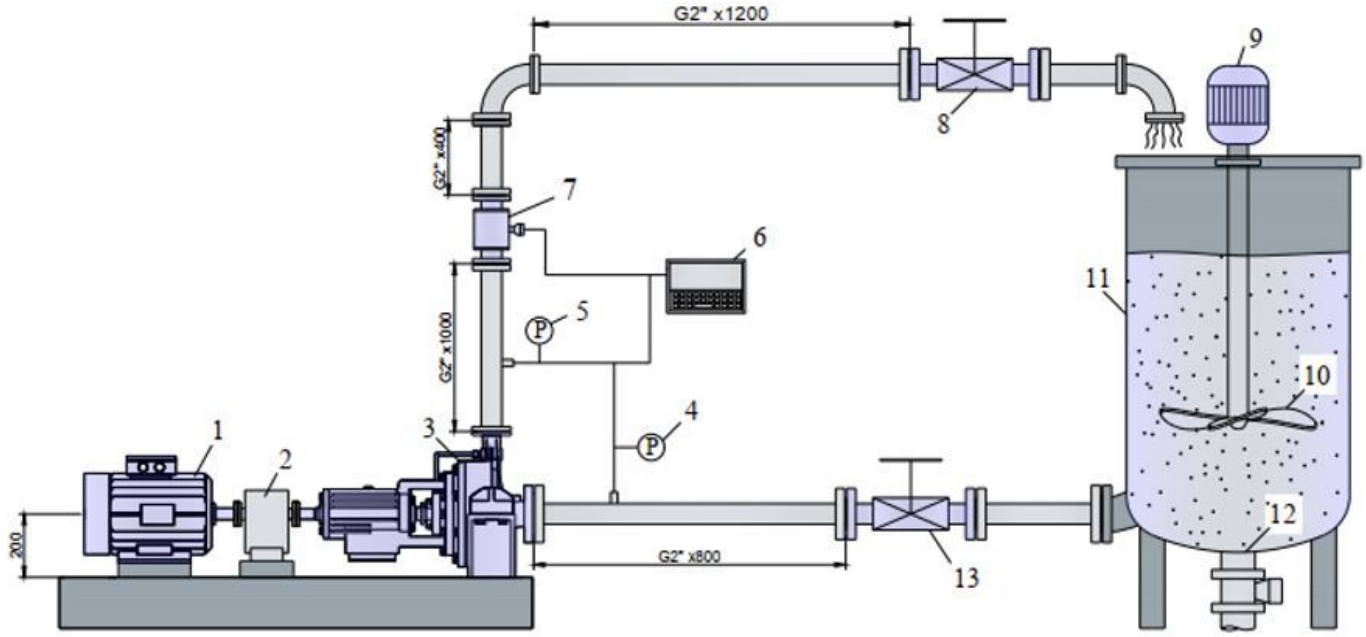

1. Electro Motor
2. Coupling
3. Centrifugal Pump
4. Suction Pressure Transducer
5. Discharge Pressure Transducer
6. Data acquisition System
7. Magnetic Flow Meter
8. Discharge Valve
9. Mixer Motor
10. Mixer
11. Test Tank
12. Drain Valve
13. Suction Valve

Figure 4

Testbed schematic (all dimensions are in millimeter)

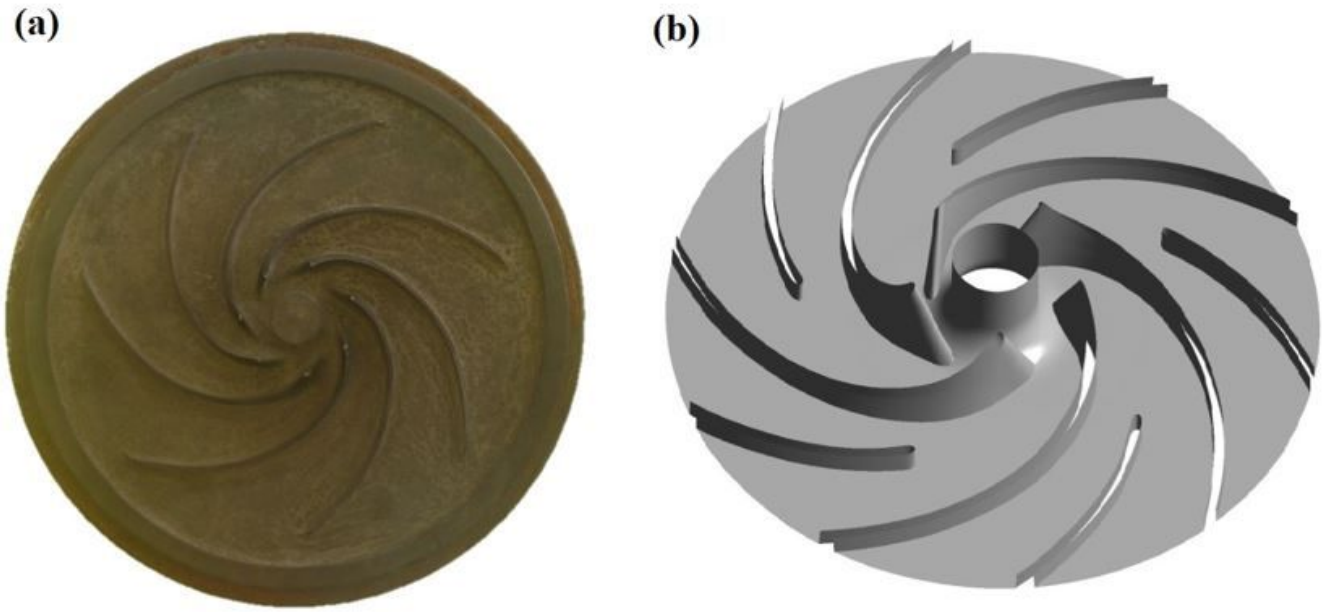

Figure 5

(a) Impeller geometry of selected case study and (b) new impeller with the splitter

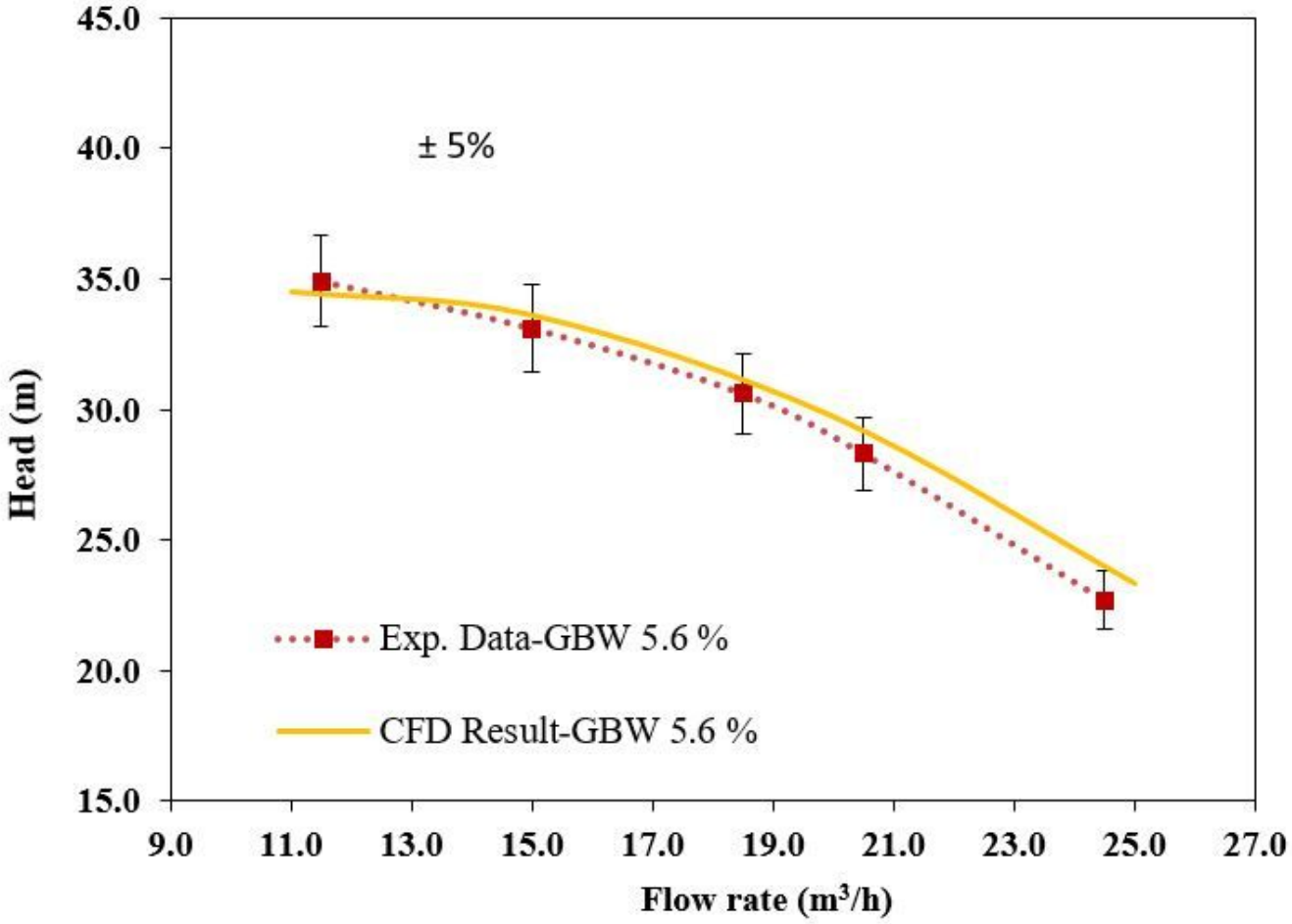

Figure 6

Comparison of the numerical simulation results (yellow line) with experimental data (red line) for GBW slurry at a concentration of 5.6%

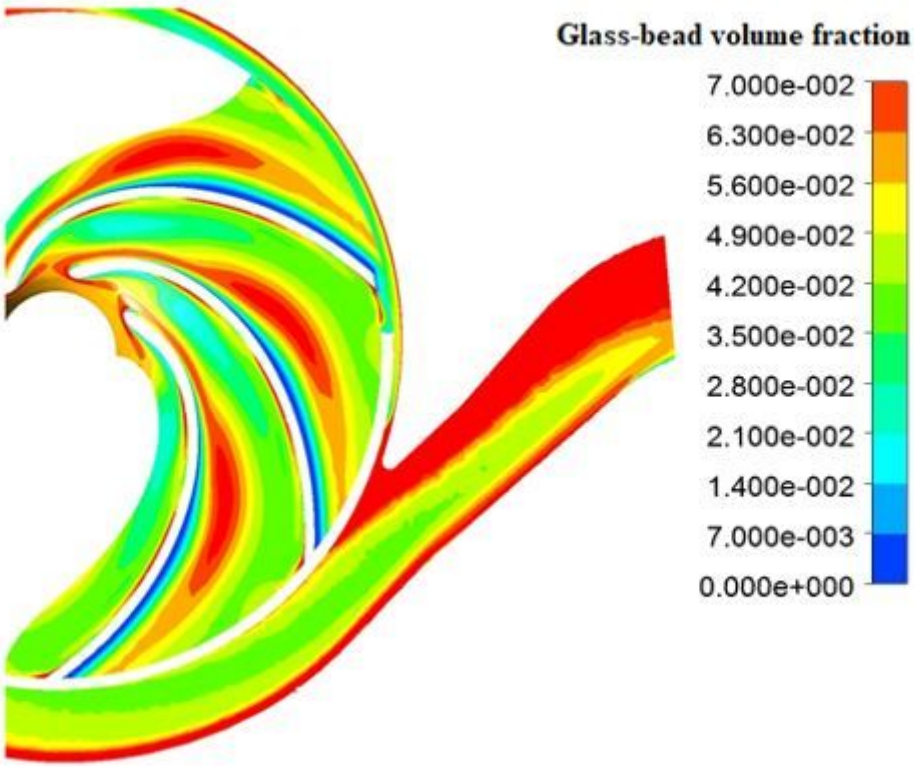

Figure 7

Distribution of particles volume fraction in the GBW slurry at a concentration of 5.6%

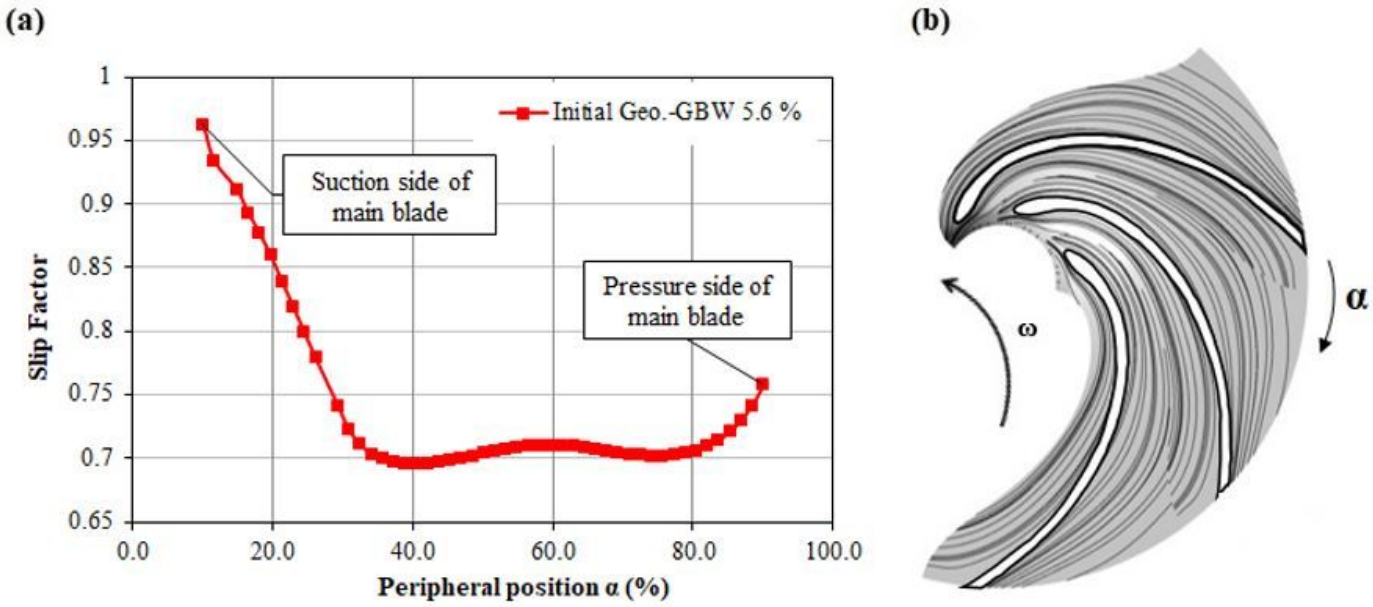

Figure 8

Distribution of slip factor in the GBW slurry at a concentration of 5.6% in the initial impeller

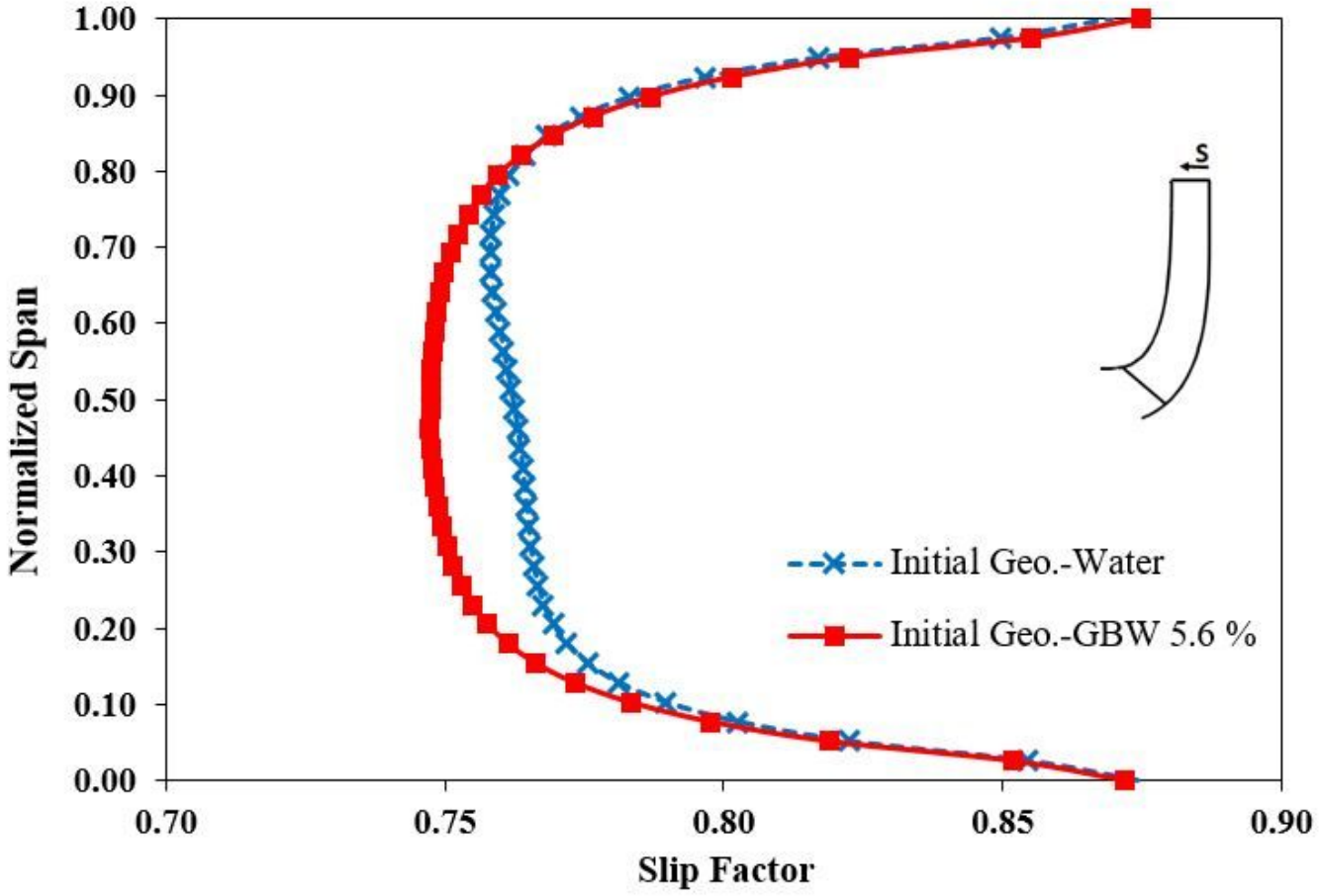

Figure 9

Comparison of the slip factor in the blade height direction from hub to shroud for water and GBW 5.6% slurry

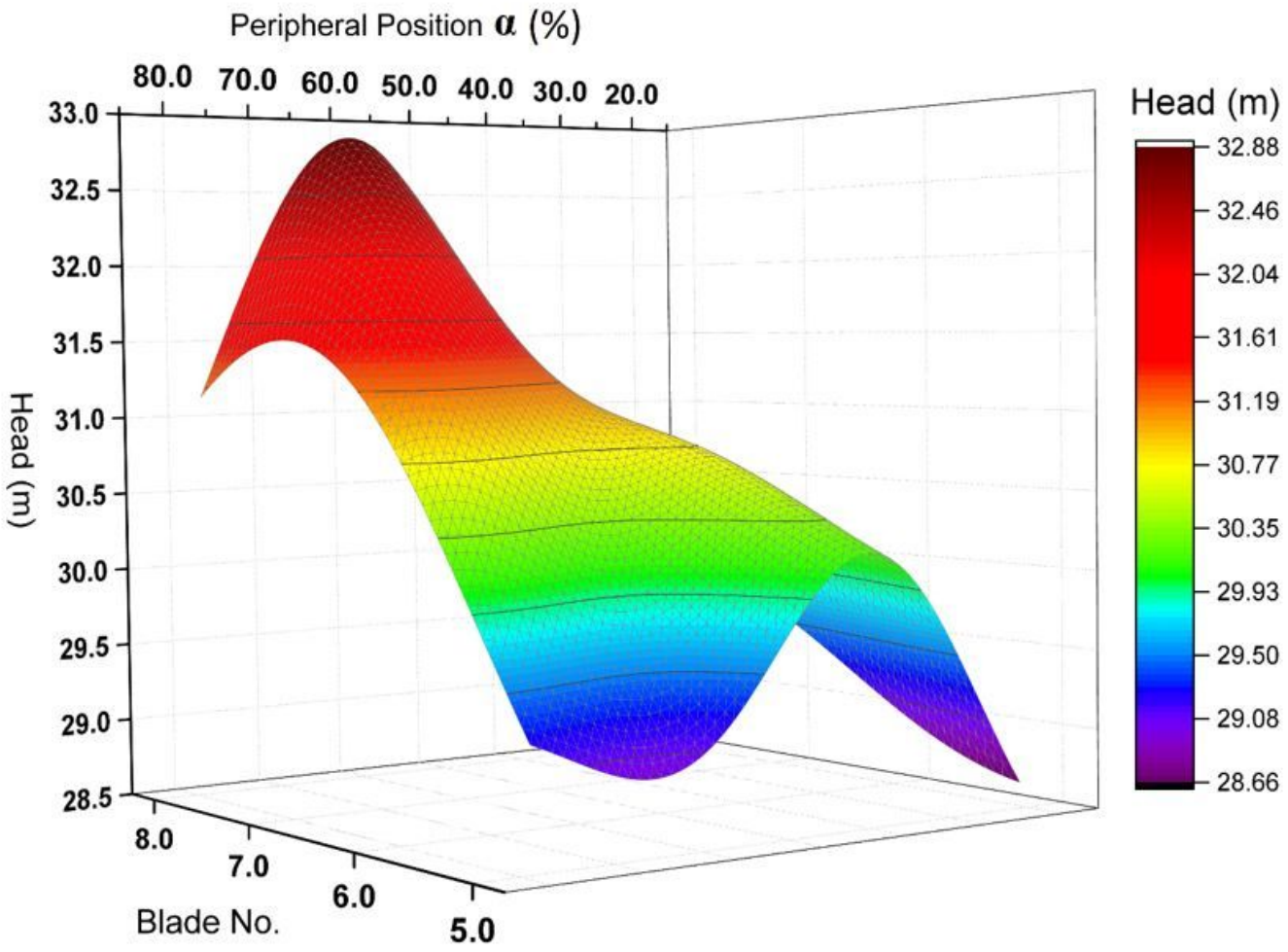

Figure 10

Effect of splitter blade number and peripheral position on the head

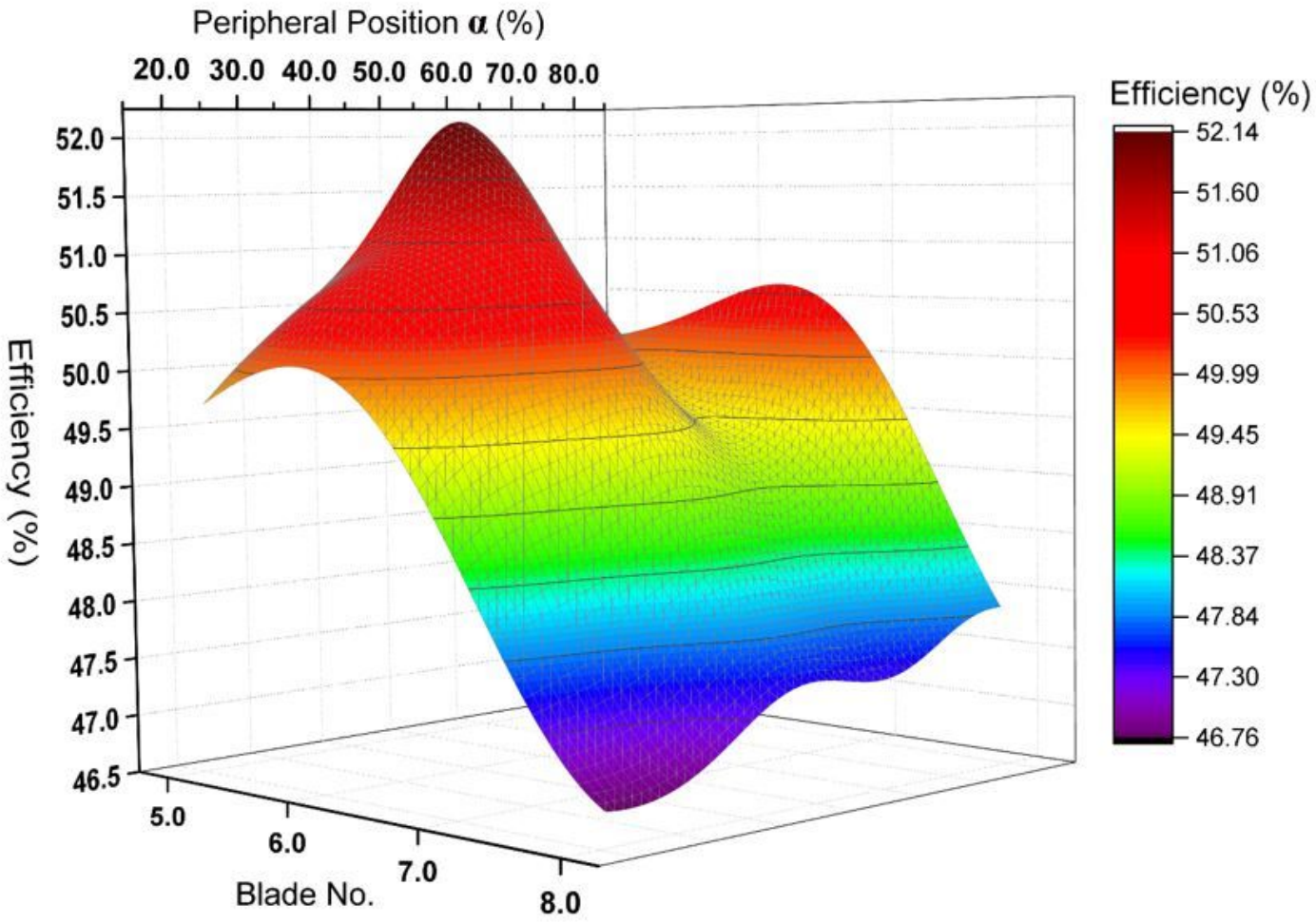

Figure 11

Effect of splitter blade number and peripheral position on efficiency

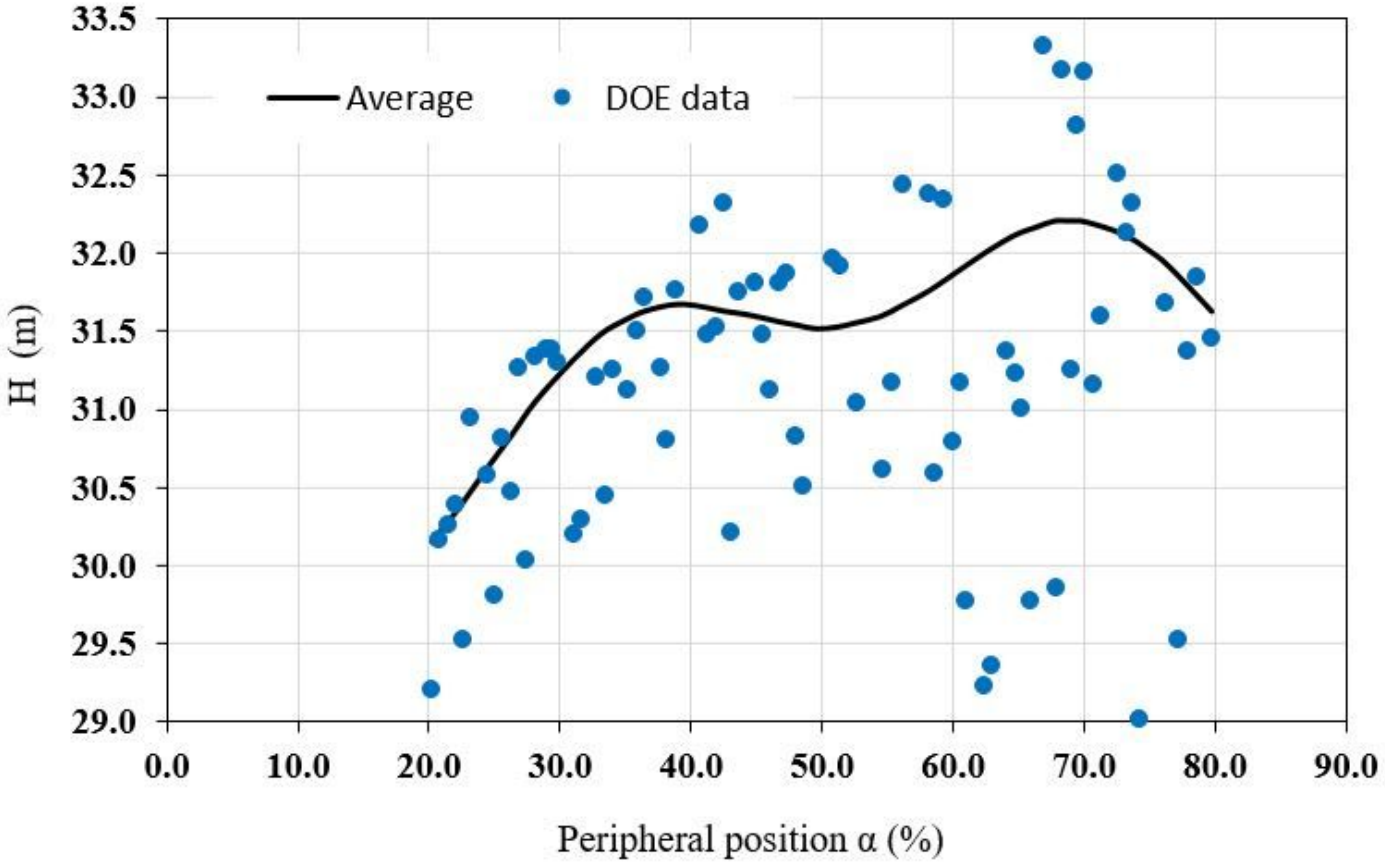

Figure 12

Effect of splitter blade position on the head

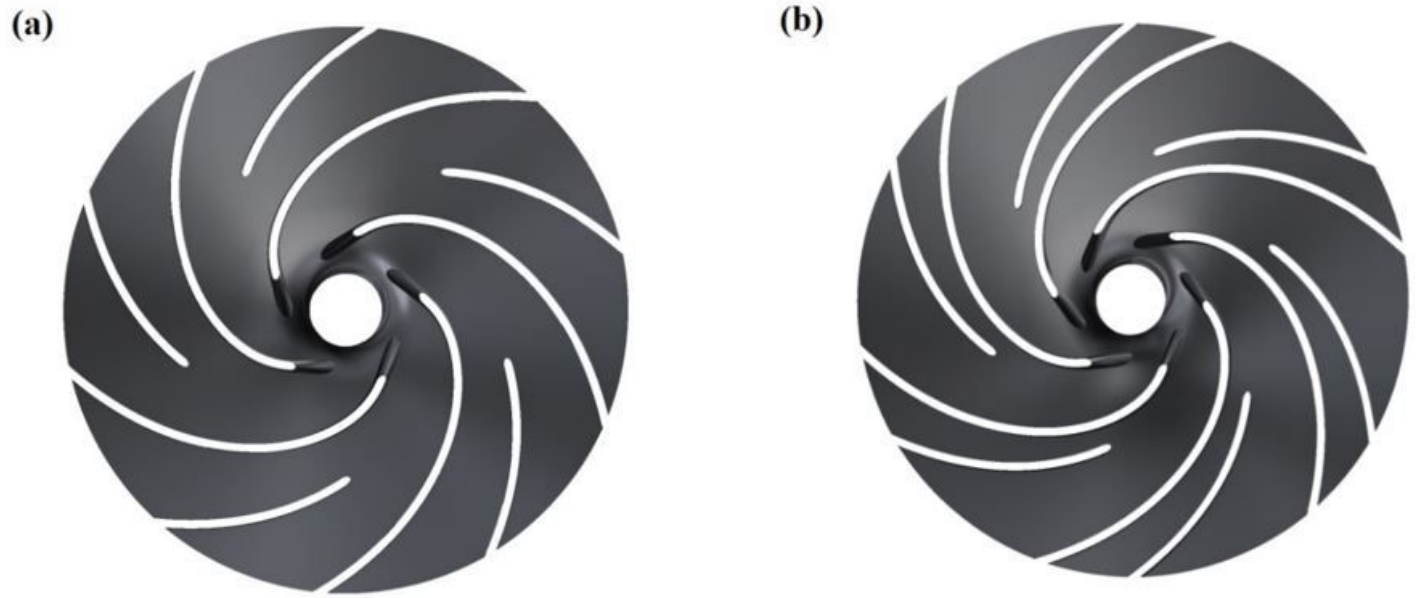

Figure 13

Comparison of primary (a) and optimal geometry (b) of the impeller in the optimization process

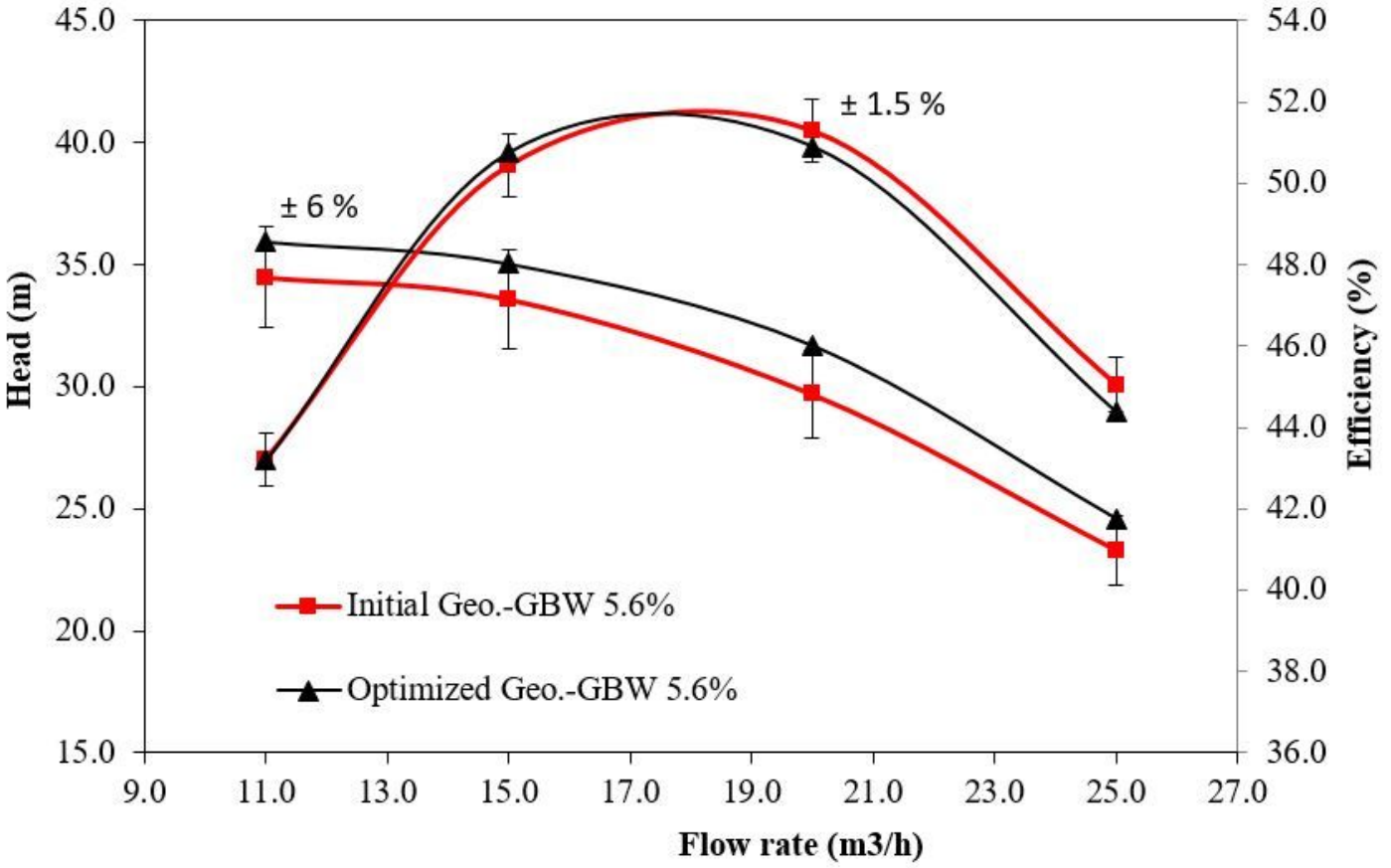

Figure 14

Comparison of head and efficiency in the initial and optimized impeller

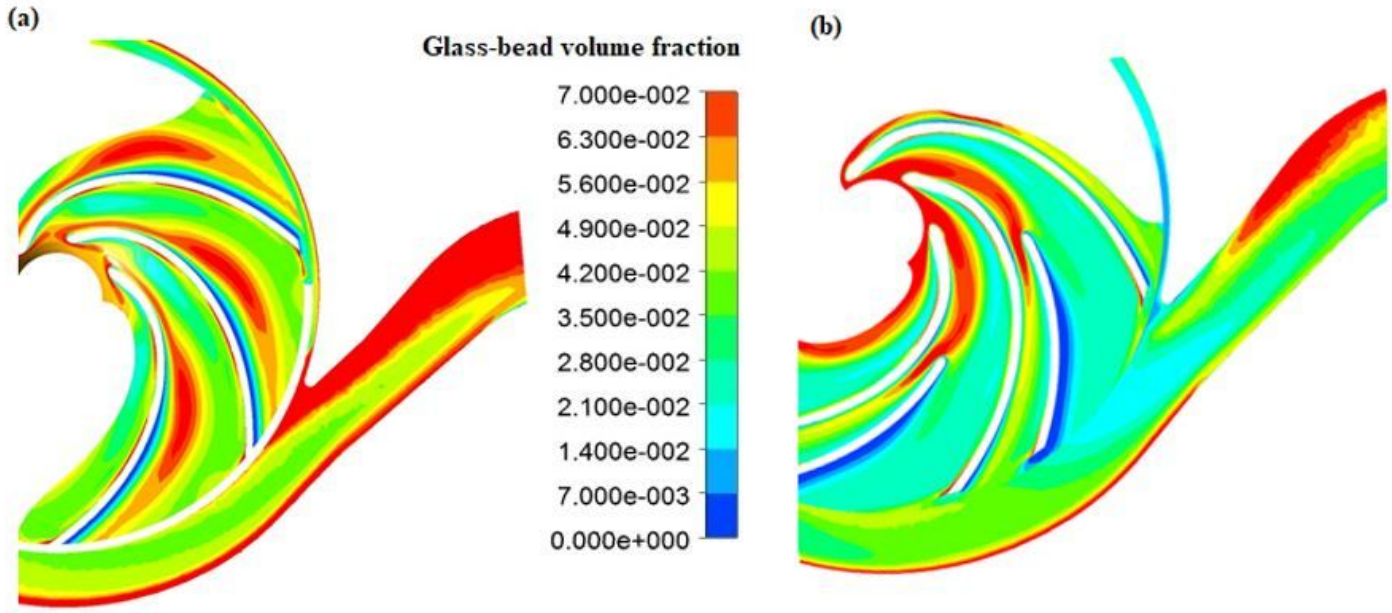

Figure 15

Comparison of solid distribution in the initial and optimized impeller

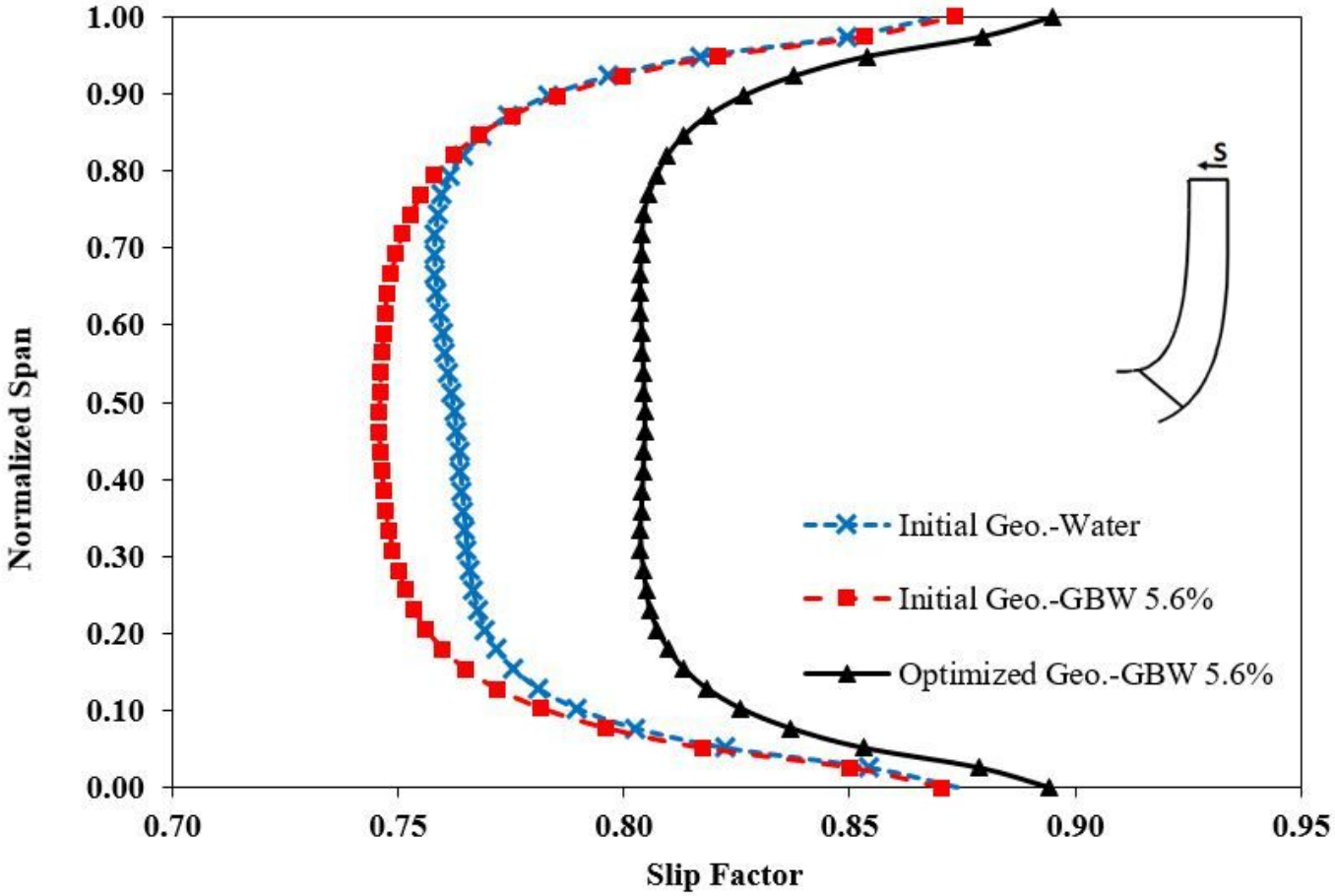

Figure 17

Height distribution of slip factor in optimized impeller from hub to shroud

Supplementary Files

This is a list of supplementary files associated with this preprint. Click to download.

- supplementarymaterial.docx